2008

Electrochemistry of pyrenyl iron terpyridines on glassy carbon, gold, and CNT

Hsiao-Chu Lin
San Jose State University

ELECTROCHEMISTRY OF PYRENYL IRON TERPYRIDINES ON GLASSY CARBON, GOLD, AND CNT

A Thesis

Presented to

The Faculty of the Department of Chemistry

San Jose State University

In Partial Fulfillment

of the Requirements for the Degree

Master of Science

by

Hsiao-Chu Lin

August 2008

APPROVED FOR THE DEPARTMENT OF CHEMISTRY

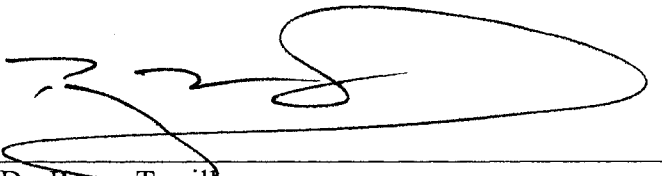

Dr. Roger ~~Terrill~~

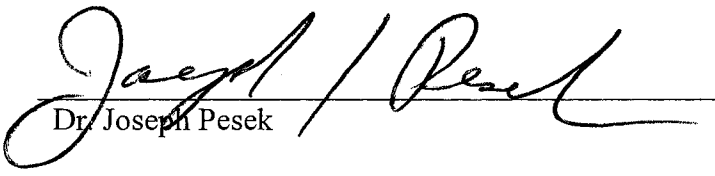

Dr. Joseph Pesek

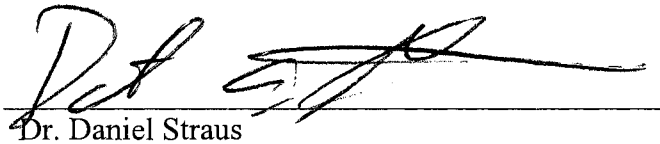

Dr. Daniel Straus

APPROVED FOR THE UNIVERSITY

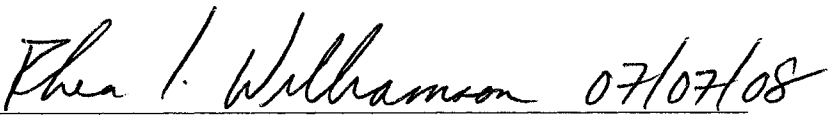

ABSTRACT

ELECTROCHEMISTRY OF PYRENYL IRON TERPYRIDINES ON GLASSY CARBON, GOLD, AND CNT

by Hsiao-Chu Lin

An iron bis-terpyridine complex bearing pyrene groups on each ligand was studied to evaluate its utility as a surface modifier of carbon nanotubes in a sensing configuration. Immersion of carbon electrodes into solutions of the complex and then into clean electrolyte established that $Fe(tpySCH_2\text{-}pyr)_2(OTF)_2$ will strongly physisorb onto glassy carbon at near monolayer coverage. But voltammetric scanning in solutions of the pyrenyl iron compound showed well-resolved Fe(II/III) redox waves that grew in magnitude over time and persisted in fresh complex-free electrolyte indicating a surface electropolymerization reaction. Very thin CNT coatings slightly increased current responses. Spectroelectrochemical analysis of $Fe(tpySCH_2\text{-}pyr)_2(OTF)_2$ films grown on indium-tin oxide transparent electrodes confirm the presence of an Fe(II/III) active redox film that has a nearly Nernstian response, but with a small Fe(II) electroinactive component.

TABLE OF CONTENTS

LIST OF TABLES

LIST OF FIGURES

1. INTRODUCTION

1.1. Research Objective

The objective of this research is to study the adsorption of a pyrene-modified redox probe to various surfaces using electrochemical methods and to evaluate its utility as a surface modifier of carbon nanotubes (CNTs) in a sensing configuration. In this research, an iron bis-terpyridine complex bearing two pyrene groups was studied by comparison with pyrene-free control compounds. The pyrenyl iron bis-terpyridine compound is expected to adsorb on various electrode surfaces, and electrochemical experiments were carried out to evaluate this hypothesis. The long-term goal of this research is to utilize this interaction to modify CNTs so they can function as electrochemical sensors using both interfacial redox electrochemistry and CNT electronic conductivity. A brief review of carbon nanotubes and electrochemical sensing is below, followed by a description of the experiments.

1.2. Carbon Nanotubes

Because of their unique properties, CNTs have gained great attention of scientific research in various areas[1] ever since their discovery in 1991 by Iijima. The structure of a CNT can be seen as a roll up of layer(s) of graphene sheet(s) into a seamless cylinder with a diameter in nanometer and length in microns. CNTs can be categorized into single-walled (SWNTs) and multi-walled (MWNTs) varieties based on the number of graphene layers inside the tubes. General properties of CNTs include light weight, small size, high mechanical strength, large surface area and high electrical conductivity.

Depending on the geometric detail of how a graphene sheet is rolled into a cylinder, the resulting SWNT may be metallic or semi-conducting. Because MWNTs are formed by multi-layers of concentric graphene sheets and each graphene sheet may have different orientation as it rolls up into a tube, the properties of MWNTs are more complicated to characterize.[2] Just like carbon fibers, CNTs exhibit high tensile strength and great resilience. They are composed exclusively of highly stable C-C which contributes to the high tensile strength of a SWNT – ~45 GPa – which is much higher than that of high-strength steel alloys (~2 GPa). They are also elastic and can be bent over a large angle and return to their original shapes without breaking. The resilience of CNTs is related to their inner diameter and geometry. CNTs with smaller inner diameter have more flexibility than the larger ones. All atoms on the CNT are covalently bonded with sp^2 geometry to neighboring C atoms and there are no unpaired electrons or dangling bonds on the CNT surface. Therefore, CNTs show a high level of chemical stability. Because CNTs are highly crystalline, they also have greater thermal conductivity along their long axis than other crystalline carbon materials like pyrolytic graphite and diamond.[1,3,4]

The exceptional properties of CNTs have generated great potential for applications in nano-scale electronic and mechanical devices. They can be applied as conducting nanowires, field effect transistors,[5,6] field emitters,[7] embedded components in composite materials,[8] hydrogen and ion storage systems,[9] nanotweezers and probes for scanning microscopes.[10] CNTs are also excellent materials for sensing or working electrochemical electrodes because in addition to the aforementioned, they possess good electrochemical stability (wide operational potential window), a selectively high surface activity, and a

large surface area. CNTs as electrode materials can achieve fast electron transfer rates, high electrocatalytic effect and enhanced sensing capabilities.[11-13]

CNT field effect transistors (CNT-FETs) utilized in sensing configurations have attracted much attention in developing selective, highly sensitive and fast responding miniaturized chemical sensors. CNT-FETs are formed by bridging a semi-conducting SWNT between two metal contacts as source and drain. In these applications a semi-conducting SWNT serves as a channel for current to flow through when a voltage is applied to the gate electrode. Upon the exposure to a target analyte, the current that flows through the SWNT changes. This change in resistance and conductivity can be measured and CNTs can then be utilized as electrochemical sensor material using CNT electronic conductivity. Kong et al[14] has demonstrated the use of SWNTs as sensitive and fast responding chemical sensors for NO_2 and NH_3.

1.3. The Use of CNT as Working Electrode Modifier

Conventional solid electrodes, such as gold, platinum and glassy carbon, can be applied to chemical sensing problems in different solvent systems and potential ranges. However, conventional bare electrodes may be inefficient for any of the following reasons: (1) the electrodes are inactivated by unwanted material precipitated or adsorbed on their surface which affects their sensitivity and reproducibility, (2) some analytes transfer electrons too slowly to electrodes and so require excessive overpotential to drive the reaction at a measurable rate, (3) unmodified electrodes are limited to use with electroactive analytes.[15]

In order to improve the deficiency of bare electrodes and extend their applications as analytical tools, chemically modified electrodes (CMEs) have been developed since the mid-1970s.[15] CMEs are prepared by attaching a chemical species, called a modifier, onto the surface of bare electrodes. By immobilizing the modifier on their surfaces, CMEs are expected to have the capability of the bare electrodes with the properties of the modifier in order to achieve superior performance. Besides the composition of the modifier, the substrates of CMEs must be carefully chosen for chemical stability. Since the reaction occurs on the interface between electrode and electrolyte solution, the area and shape of the electrode surface also affect the reaction rate and the capability of CMEs.[16] The general approaches of attaching the modifier to the electrode surfaces include the following: (1) monolayer adsorption, (2) covalent bonding, (3) polymer modification, (4) heterogeneous multimolecular layers.[15,16]

1.4. Electrochemical System

Electrochemistry is the science which studies the electron and charge transfer when a chemical reaction occurs. An electrochemical reaction is a reaction that takes place when the energy of electrons on the surface of an electrode is altered by an applied voltage that makes the electron transfer occur between an electroactive species and the electrode. When a voltage is applied, it supplies electrical energy and this changes the energy of electrons on the surface of the electrode. An oxidation reaction occurs when the electrons are transferred from the electroactive species to the electrode (anode), usually when it is biased positively, and a reduction reaction occurs, usually under negative bias, when electrons are transferred from the electrode (cathode) to the

electroactive species. Since electron transfer is the driving force for many chemical reactions, electrochemistry offers the potential to study these processes by mentoring the electrons involved that may not be achieved by other analytical techniques.

The three-electrode cell is the most commonly used electrochemical system, which includes a working electrode, a reference electrode and an auxiliary electrode which are immersed in an electrolyte solution.[16,17] The potential of the working electrode is controlled relative to that of the solution as sensed by the reference electrode. Control is achieved in a feedback configuration in which a current supplied through the auxiliary electrode is controlled by the potential measured by the reference electrode. The working electrode is the one at which the reaction under study takes place. Both liquid mercury electrodes and solid electrodes are often used. The oldest of these electrochemical methods is known as polarography and utilizes a mercury electrode – polarography was invented by Jaroslav Heyrovsky.[18] The mercury electrode has the advantages of possessing a large cathodic potential window due to its high hydrogen overvoltage and it can be used without special pretreatment. However, mercury is a toxic and easily oxidized material and it will lose its electroactivity when the applied voltage is even slightly positive.[17] Therefore, the application of mercury electrode is limited by its operating anodic potential range.

Solid electrodes, on the other hand, overcome this disadvantage of mercury and can be made of various inert materials, such as platinum, carbon, gold and silver. Electrodes made of different materials have slightly different potential windows. The surface of a solid electrode can be modified to increase its sensitivity, selectivity and stability and the

modified electrodes can be employed in various electrochemical applications. The surfaces of solid electrodes normally need to be polished to remove any residue adsorbed on the surface that may affect the results before carrying out experiments.[16,17,19]

The reference electrode is used to accurately control the potential of the working electrode, so within the detecting current range, the potential of an ideal reference should remain constant. Therefore, it is important to select a stable, reproducible and easily calibrated reference electrode in order to keep the potential constant during the experiment. The saturated calomel electrode (SCE) and saturated silver chloride electrode (Ag/AgCl) are commonly used aqueous reference electrodes.

The main function of an auxiliary electrode is to maintain the electrical neutrality of the solution during the electrochemical reaction. The polarity of the auxiliary electrode changes according to the demands of the potential that is programmed at the working electrode. Under proper conditions the auxiliary electrode will be effectively invisible and will not affect the working electrode in any way. The most commonly used auxiliary electrode material is platinum.[16,17]

1.5. Cyclic Voltammetry

Cyclic voltammetry (CV) is one of the electrochemical techniques used to study the redox reaction of a molecule. In CV, a variable voltage is applied to the working electrode and the current response is measured and expressed as a function of potential. The voltage applied to the working electrode is determined by setting the initial potential (IP) and the switching potentials, V1 and V2. In the forward scan, the voltage applied to the working electrode starts from IP and increases linearly until reaching the first

switching potential, V1, and is followed by a reverse scan, in which the variable potential scans linearly back to a second switching potential, V2. The current responses produced by the electron transfer between the working electrode and the molecule in solution are measured, and the results are recorded in a cyclic voltammogram which is expressed as current versus corresponding potential. Figure 1 shows an excitation signal waveform for CV and a resulting cyclic voltammogram.[16,17] For CV, the variable potential excitation signal shows a triangular potential waveform, and the scan is cycled between the two switching potentials.

1.5.1. Electrode Reaction

The *Randles-Sevcik equation* can be used to calculate the cyclic voltammetry response in the form of the peak current that will theoretically be observed for a reversible couple if the electrode reaction is diffusion-controlled. The *Randles-Sevcik equation* is expressed as[16,17]

$$\text{At } 25^{\circ}\text{C}, \qquad i_p = \left(2.69 \times 10^5\right) \cdot n^{3/2} \cdot A \cdot D^{1/2} \cdot C \cdot \upsilon^{1/2} \tag{1}$$

where

i_p = peak current

F = Faraday constant = 94853 C mole^{-1}

n = number of electrons transferred

A = the surface area of electrode (cm^2)

D = diffusion coefficient of the analyte in solution (cm^2 s^{-1})

C = concentration of the analyte (mol cm^{-3})

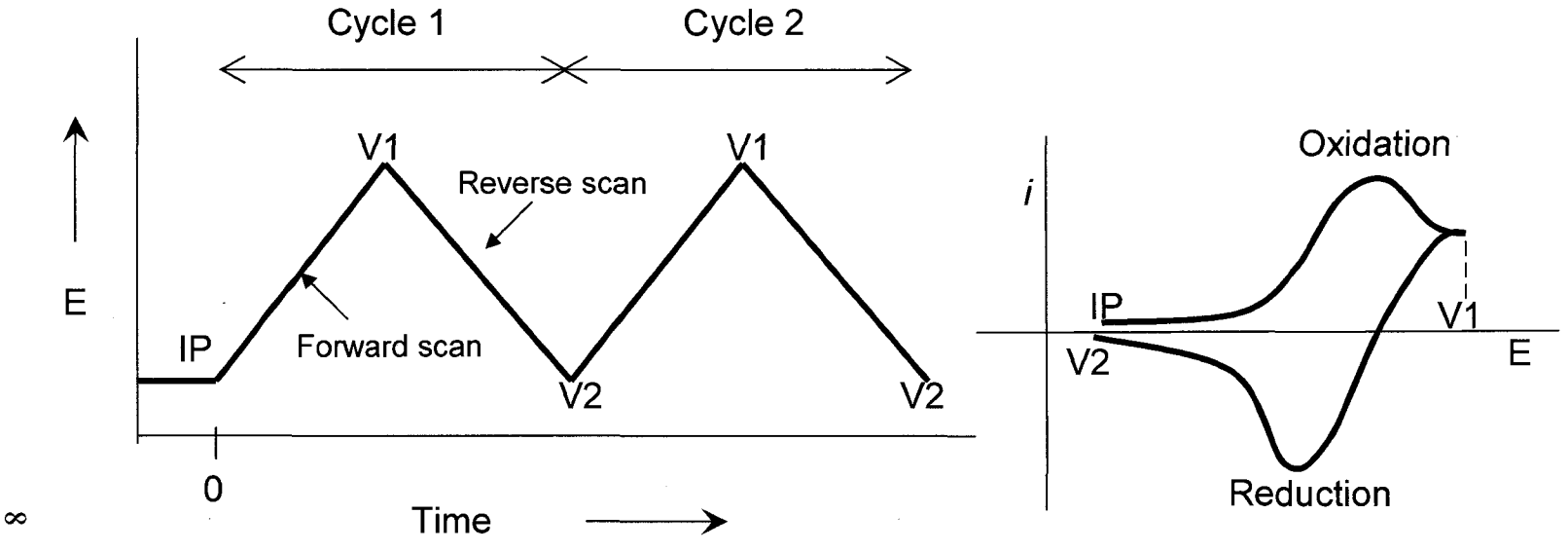

Figure 1. (a) Cyclic potential sweep excitation signal; (b) Resulting cyclic voltammogram.

υ = scan rate (V s^{-1})

R = gas constant = 8.31447 J K^{-1} mol^{-1}

T = temperature (K)

From the equation, the peak current response of a diffusion-controlled reaction is determined by the area of electrode surface, diffusion coefficient and concentration of the species, the number of electrons transferred in the reaction and the scan rate of the system.

In a cyclic voltammetry experiment, if the electrode reaction is "adsorption-controlled" – that is, the species undergoing electron transfer are immobilized at the electrode surface and do not diffuse away into solution, the cathodic wave and the anodic wave in the resulting voltammogram mirror one-another through the potential axis.[16] Moreover, the anodic peak potential (E_{pa}) equals to the cathodic peak potential (E_{pc}) for an ideal adsorption-controlled nernstian reaction and the peak current can be expressed by the *Laviron equation*:[16,17,20]

$$\text{At 298 K,} \qquad i_p = \left(9.39\times10^5\right)\cdot n^2\cdot\upsilon\cdot A\cdot\Gamma \qquad (2)$$

where

Γ = the surface coverage of the electrode reaction substance (mol cm^{-2})

The surface coverage of the electroactive species adsorbed on the electrode surface can be calculated from the quantity of charge (Q), which can be obtained by integrating the anodic or cathodic peak area according to the following equation:[17,21]

$$\Gamma = \frac{Q}{nFA} \tag{3}$$

The number of molecular layers adsorbed on the surface of electrode can be obtained by dividing the surface coverage of the molecule calculated from Equation 3 by the coverage of a molecular monolayer model.

From Equations 1 and 2, the relationship between the peak current and the scan rate of the reaction is observed. The peak current of an adsorption-controlled electrode reaction is proportional to the scan rate (υ), and for a diffusion-controlled electrode reaction, the peak current is proportional to the square root of the scan rate ($\upsilon^{1/2}$). Therefore, if the mass transfer of the electroactive species to the electrode surface is by diffusion, the relationship between the peak current and the scan rate will be linear. When the electroactive species adsorbs to the electrode surface and posseses fast electron transfer between the species and the electrode, then the peak current will have a linear relationship with the square root of the scan rate. These relationships can be applied to understand the surface interaction between the species and electrode and to determine whether the electroactive species adsorbs on the electrode or not.

Comparing the voltammograms for the diffusion-controlled and the adsorption-controlled reactions, the current responses at the end of the forward scan show different characteristics. For a diffusion-controlled reaction, the current response at the end of the forward scan does not go to zero because molecules in the solution can still diffuse to the electrode surface and supply a diminishing current response. But in an adsorption-controlled reaction, the electroactive molecules in the solution are fixed at the electrode

surface and so can be exhaustively oxidized and in which case the current response goes to zero. Therefore, the current response at the end of the forward scan goes to zero for an adsorption-controlled reaction.

1.6. Research Outline

In this study, three iron bis-terpyridine compounds were studied electrochemically using glassy carbon, gold and CNT-coated electrodes. The structures of the three iron compounds are shown in Figure 2 – two act as controls and the third structure bears two pendant pyrene units that are anticipated to promote their adsorption onto graphitic materials. The experiments are designed around a simple question – do the complexes adsorb to the electrode surface? The adsorption of the compound onto the electrode surfaces was evaluated with a series of CV experiments that use the following protocol: first, the electrode was immersed in an electrolyte solution containing the dissolved complex and in most cases it was subjected to repeated electrochemical scans. Following the scans a fresh electrolyte solution without the dissolved complex was exchanged into the cell and the experiments were repeated – the obvious expectation being that the response will disappear unless the complexes adsorb strongly. Scan rates studies before and after the exchange were used to support the conclusions regarding adsorptive behavior.

For those cases where adsorption of the compound on electrode surfaces was confirmed, the adsorption phase was studied in more detail by examining the effect of CV scanning and immersion time on the growth of molecular films. In these experiments we sought to distinguish between two mechanisms for the accumulation of complex at

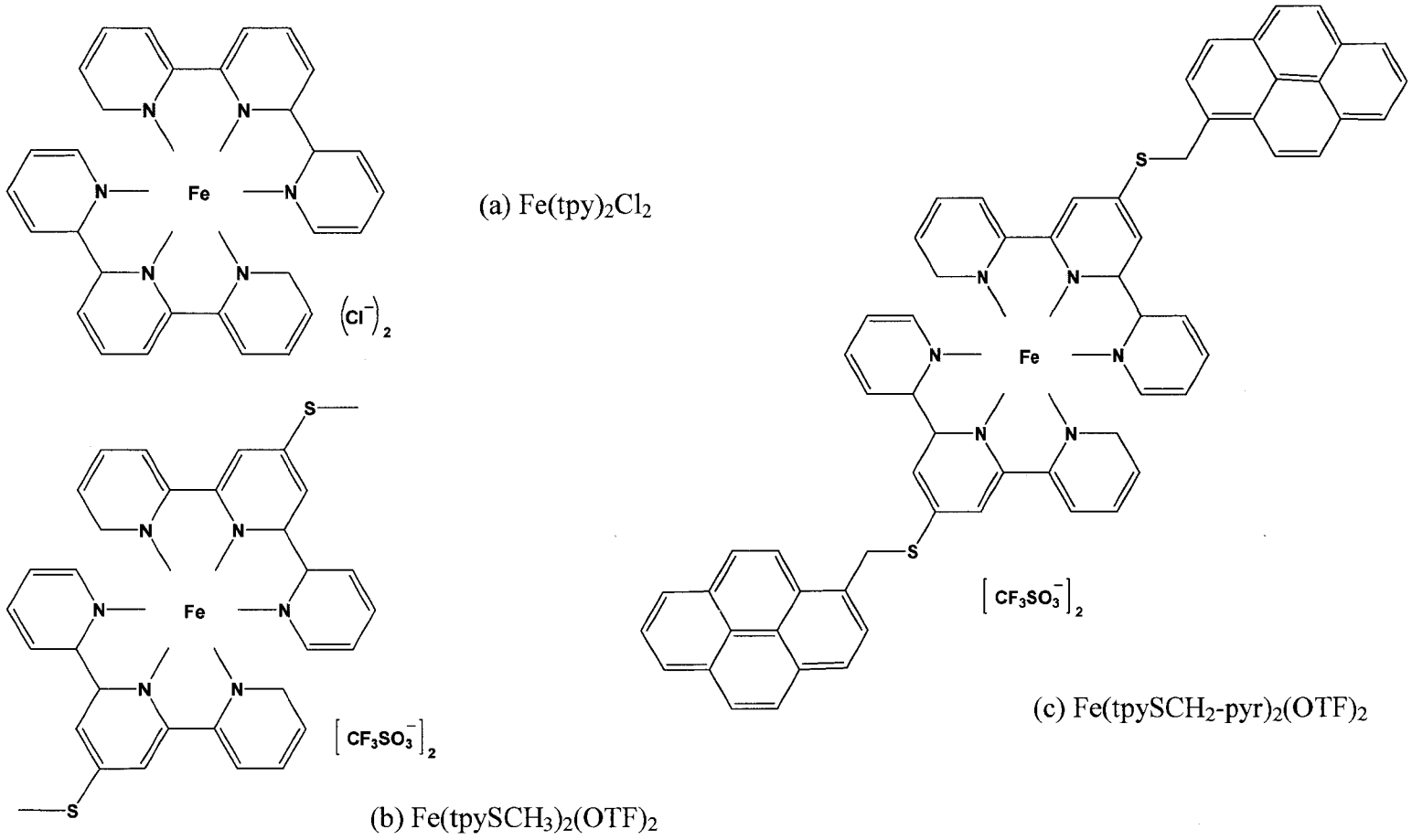

Figure 2. Molecular structures of three bisterpyridine iron compounds being analyzed: (a) $Fe(tpy)_2Cl_2$; (b) $Fe(tpySCH_3)_2(OTF)_2$; and (c) $Fe(tpySCH_2\text{-}pyr)_2(OTF)_2$

the surface – our question was this: does electrochemical scanning during the adsorption phase influence the amount of adsorbed material that is finally observed? In these experiments three identical GC electrodes were immersed in electrolyte containing the Fe-complex to begin the accumulation process. One electrode was scanned frequently during the adsorption phase (every minute for 60 minutes), another was scanned just once immediately upon immersion and then again after 60 minutes, and a third was not scanned at all during the adsorption phase. Lastly, a spectroelectrochemical experiment was also carried out using UV-Vis spectroscopy to study the extent of Fe(II)/Fe(III) oxidation and the results were compared with an ideal Nernstian response.

2. EXPERIMENTAL

2.1. Chemicals and Reagents

The iron terpyridine compounds (structures shown in Figure 2) were prepared by Dr. Daniel Straus at San Jose State University using a synthetic procedure of his own design. The solvent used to run all the electrochemical experiments was HPLC grade acetonitrile purchased from Riedel-de Haen and the supporting electrolyte was high purity lithium perchlorate and was purchased from Aldrich. Multi-walled carbon nanotubes (MWNTs) were purchased from Aldrich. N,N-dimethylformamide (DMF) used as solvent for CNT suspension was from Mallinckrodt Chemcial.

2.2. Electrochemistry System

The electrochemical setup used was a conventional three-electrode cell which included a working electrode, a silver wire quasi-reference and a platinum wire auxiliary electrode. The electrochemical experiments were performed using an EG&G Princeton Applied Research (PAR) Potentiostat/Galvanostat Model 273 and PAR Model 270 Electrochemistry Software.

2.3. Working Electrode Preparation

Various working electrodes were used to run the electrochemical analyses, including glassy carbon (GC) electrode with a diameter of 2 mm, gold electrode with a diameter of 1.5 mm and GC and Au electrodes coated with carbon nanotubes (CNT). In order to clean the electrode surface, GC and Au electrodes were first washed with soap and distilled water, rinsed with ethanol, then polished with 0.3 micron aluminum oxide (Buehler) on TexMet® polishing cloth followed by ultrasonic agitation in water.

The preparation of CNT coatings on the electrodes followed the procedure described in the work of Wang, et al.[22] A solution of CNT was made from dispersing 1 mg of MWNTs in 10 mL of N,N-dimethylformamide (DMF) followed by ultrasonic agitation to form a black supernatant. To coat the electrode surface with CNT, a 15 μL droplet of CNT supernatant in DMF was deposited onto the electrode surface and the solvent was evaporated using medium heat gun with flow directed directly onto the surface along the surface normal. This process was then repeated once to yield a thin CNT coating.

2.4. Spectroelectrochemical Analysis

Spectroelectrochemical analysis was done by coupling the electrochemical setup to a UV-Vis spectrophotometer in order to monitor the change in absorbance responding to different voltages applied. The spectroelectrochemical experiments were done at room temperature using a PAR Potentiostat/Galvanostat Model 263A and Model 270 software and using a Cary 50 Bio UV-Vis spectrophotometer. Indium tin oxide (ITO) was used as the working electrode due to its optical transparency and good electrical conductivity. A small slide of ITO on glass was fit to a silica cuvette and was held in the spectrophotometer along with a Pt wire auxiliary and Ag wire reference electrode.

3. RESULTS and DISCUSSION

3.1. $Fe(tpy)_2Cl_2$ Control at GC and CNT-coated GC Electrodes

Figure 3 shows the voltammograms of a blank solvent with electrolyte (Figure 3a) and $Fe(tpy)_2Cl_2$ (Figure 3b) at a bare GC electrode at a scan rate of 100 mV $s.^{-1}$ The CVs were first scanned with blank electrolyte solution, and a small amount of $Fe(tpy)_2Cl_2$ was added to the blank and followed by several CV scans run every 10 minutes. The solution in the cell was then replaced with a fresh electrolyte solution without cleaning the electrode surface and a CV scan was run using the same setting (Figure 3c).

Figure 4 shows an identical set of $Fe(tpy)_2Cl_2$ voltammograms, this time employing a CNT-coated GC electrode. The experimental setup, conditions and instrumental settings were the same for these two sets of experiments. A CV was scanned with a blank electrolyte solution (Figure 4a) by setting the program to IP = 0, V1 = 1.5 V and V2 = 0. After a small amount of $Fe(tpy)_2Cl_2$ was added to the cell, a series of CV scans (Figure 4b) were run every 10 minutes setting the program to IP = 0, V1 = 1.3 V and V2 = 0. Another CV (Figure 4c) was scanned after the solution in the cell was replaced with clean electrolyte solution under the same experimental setup.

At the CNT-modified GC electrode, $Fe(tpy)_2Cl_2$ shows well-defined redox waves of Fe(II)/Fe(III) with ΔE_p = 82 mV. The concentrations of $Fe(tpy)_2Cl_2$ were not controlled in these two sets of experiments – instead a small amount of pure dry complex was spiked into the original electrolyte solution and stirred to dissolve it. By using this method, it was found that the background current responses were much more controlled presumably due to the limited exposure to ambient water and oxygen. But unfortunately,

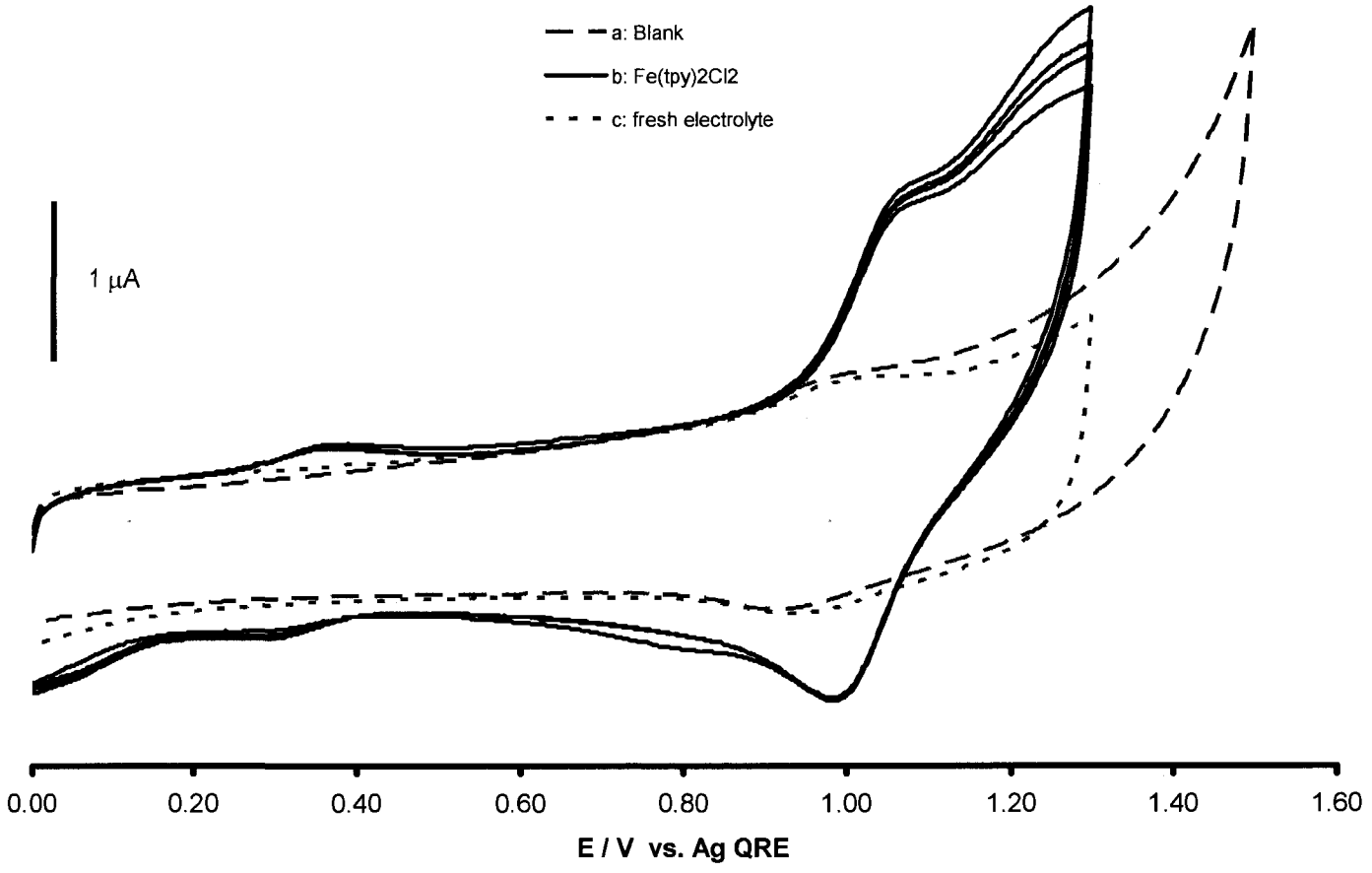

Figure 3. Cyclic voltammograms of (a) blank electrolyte; (b) $Fe(tpy)_2Cl_2$ scanned every 10 minutes; (c) fresh electrolyte exchanged into the cell at a bare GC electrode scanned 100 mV $s.^{-1}$

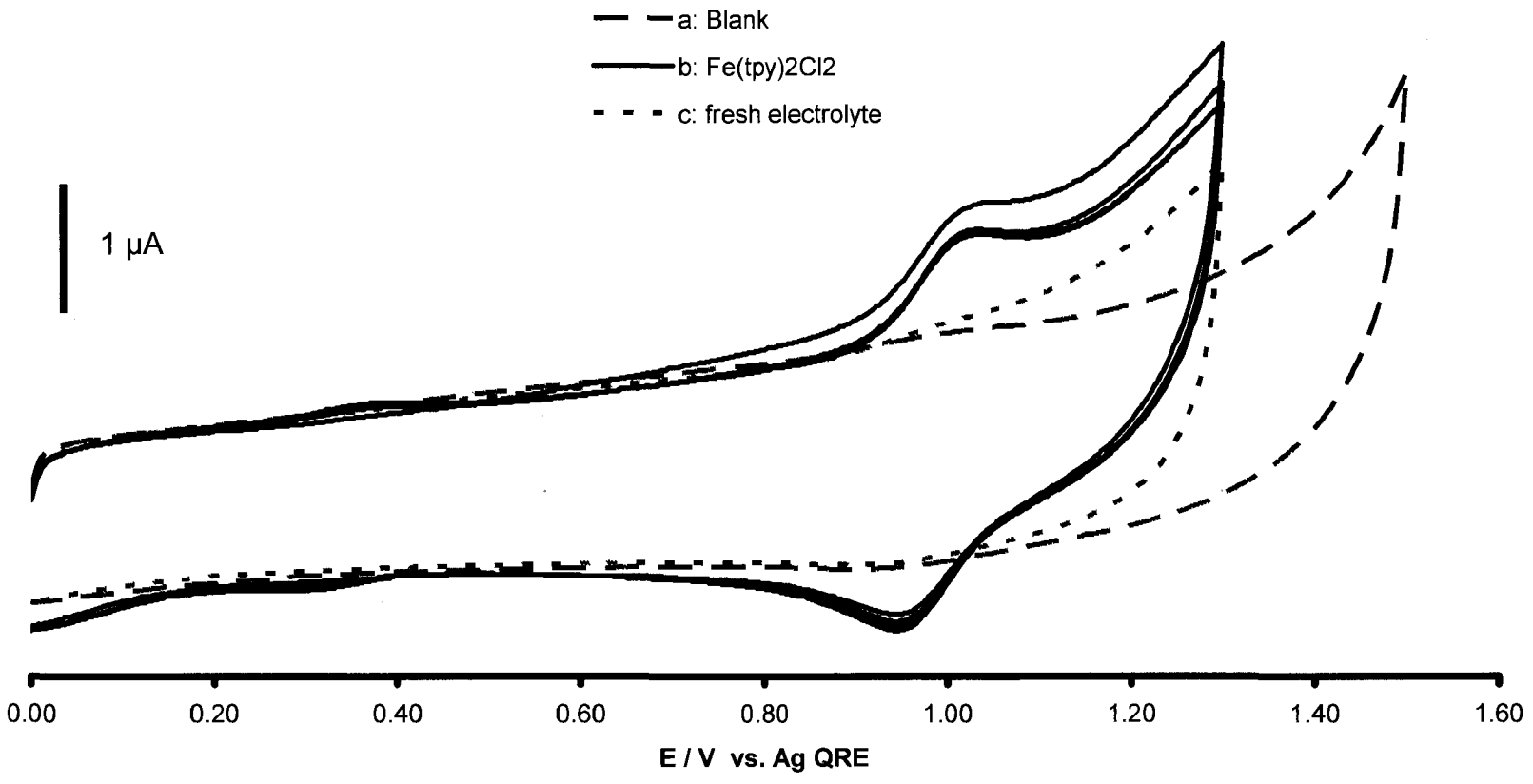

Figure 4. Cyclic voltammograms of (a) blank electrolyte; (b) $Fe(tpy)_2Cl_2$ scanned every 10 minutes; (c) fresh electrolyte exchanged into the cell at a CNT-coated GC electrode scanned 100 mV $s.^{-1}$

because of this the Faradaic current responses of the analyte in Figures 3 and 4 cannot be directly compared. The slight increase in background currents, including the charging current, observed for the CNT-coated electrode was expected due to the increase of electrode surface area by the coating of CNTs.[23] For both sets of experiments, after a clean electrolyte solution was exchanged into the cell, the current responses dropped down to the blank current levels. This suggests that the electrode reaction of $Fe(tpy)_2Cl_2$ is a diffusion-controlled process and $Fe(tpy)_2Cl_2$ adsorbs neither to GC nor CNT-coated GC electrodes. In other words, by replacing the solution, Fe complex in solution is washed away and the subsequent CV scans do not show redox waves for Fe(II)/Fe(III).

3.1.1. Scan Rate Studies

A series of CV scans were carried out in order to study the scan rate dependence of the peak current of $Fe(tpy)_2Cl_2$ at the bare GC and the CNT-coated GC electrodes and to support the observations of previous experiments. CVs of $Fe(tpy)_2Cl_2$ in electrolyte were scanned using 20, 50, 100, 200, 500 and 1000 mV s^{-1} scan rates and the resulting voltammograms are shown in Figures 5 and 6. After correcting the current response by subtracting the non-Faradaic current from the peak current, the relationship between different scan rates and the responses in peak current was plotted and shown in Figure 7.

Figure 7 shows the plots of $Fe(tpy)_2Cl_2$ current response versus scan rates at a bare GC and the CNT-coated GC electrodes. At the bare GC electrode, a power equation $i_{pa} = 0.13\upsilon^{0.49}$ was obtained. The peak current response of $Fe(tpy)_2Cl_2$ is proportional to sweep rate to the power of 0.49. At the CNT-coated GC electrode, $i_{pa} = 0.15\upsilon^{0.51}$ was obtained; peak current is proportional to sweep rate to the power of 0.51. Both plots show a trend

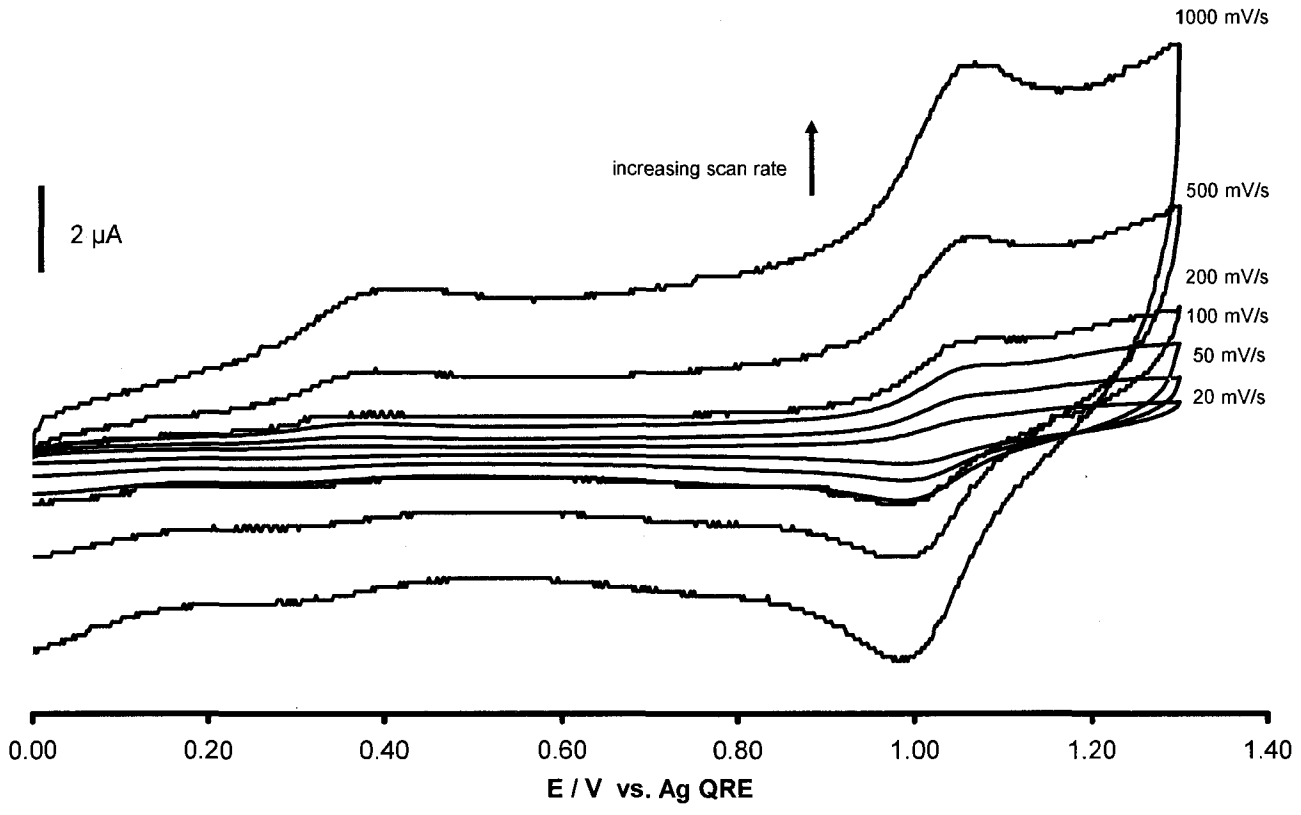

Figure 5. Cyclic voltammograms of $Fe(tpy)_2Cl_2$ at a bare GC electrode scanned from 0 to 1.3V with 20, 50, 100, 200, 500, 1000 mV s^{-1} scan rates.

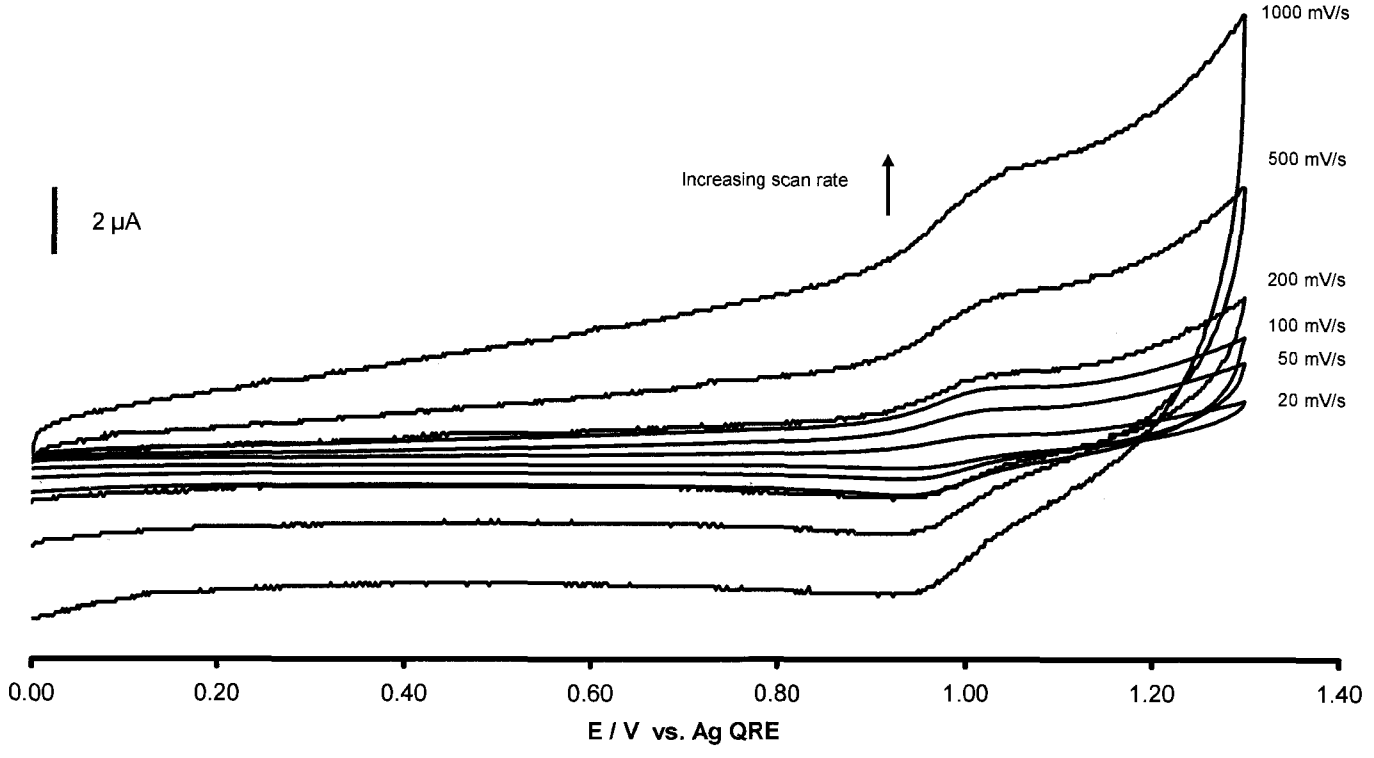

Figure 6. Cyclic voltammograms of $Fe(tpy)_2Cl_2$ at a CNT-coated GC electrode scanned from 0 to 1.3V with 20, 50, 100, 200, 500, 1000 mV s^{-1} scan rates.

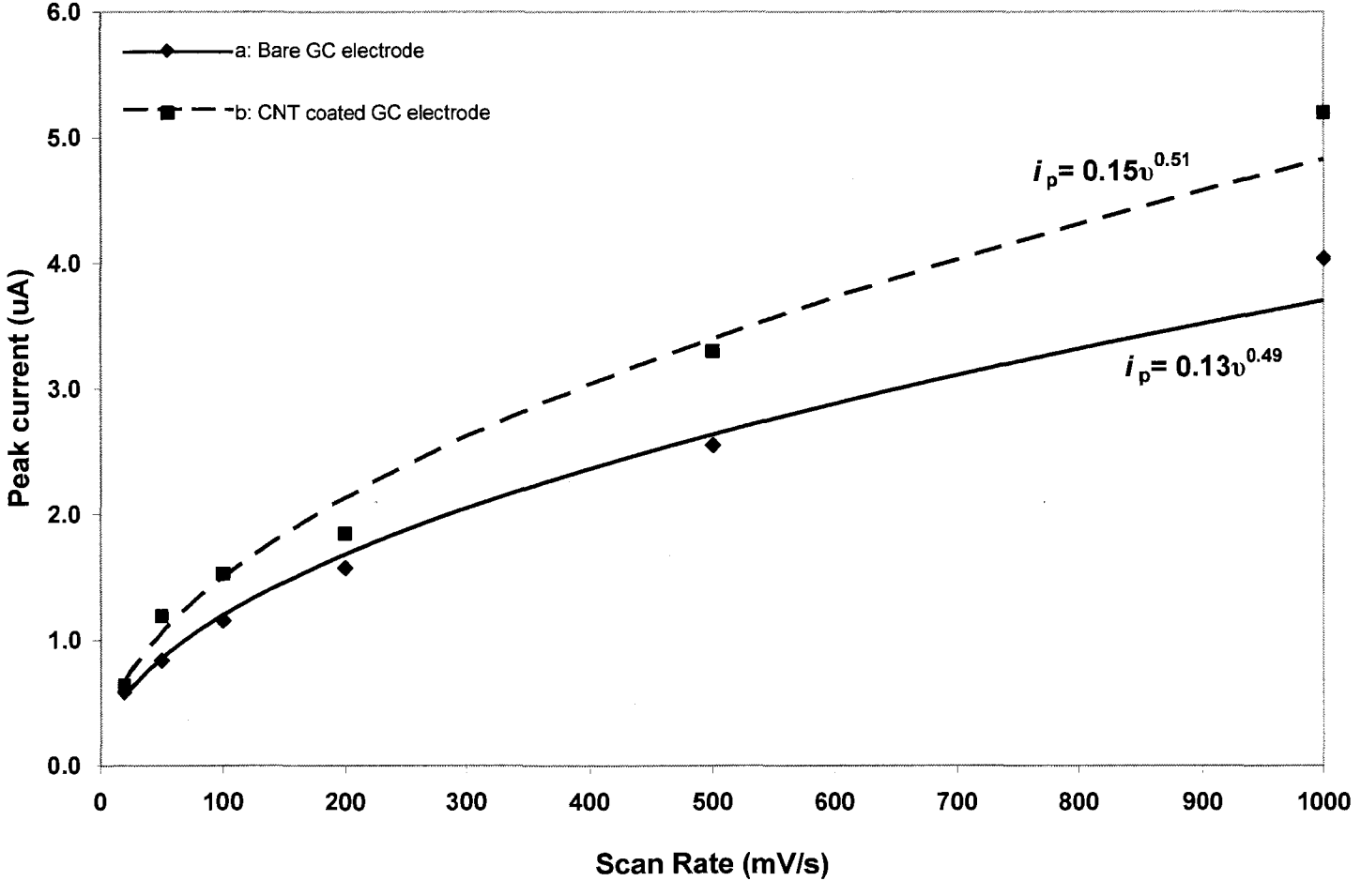

Figure 7. Sweep rate dependence of the peak current of $Fe(tpy)_2Cl_2$ at (a) a bare GC and (b) the CNT-coated GC electrode.

in which the peak current response of $Fe(tpy)_2Cl_2$ is closely proportional to the square root of the sweep rate of CV scan. According to the *Randles-Sevcik equation*, for a diffusion-controlled electrode process, the peak current is proportional to the square root of the sweep rate. This supports the earlier observations which indicate that $Fe(tpy)_2Cl_2$ exhibits a diffusing behavior and binds to neither GC nor CNT-coated GC electrode.

3.2. $Fe(tpySCH_3)_2(OTF)_2$ and $Fe(tpySCH_2\text{-}pyr)_2(OTF)_2$ at GC Electrode

$Fe(tpySCH_3)_2(OTF)_2$ (Figure 2b) and $Fe(tpySCH_2\text{-}pyr)_2(OTF)_2$ (Figure 2c) are molecules that have similar molecular structures, except for the pyrene groups attached on each terpyridine of $Fe(tpySCH_2\text{-}pyr)_2(OTF)_2$. CV was used to analyze these two molecules under the same conditions used above. The electrochemical cells were prepared with a GC working electrode, voltages were set to IP = 0, V1 = 1.3 V and V2 = 0 and CVs were scanned using a 100 mV s^{-1} sweep rate. The voltammetric responses of these two compounds are shown in Figure 8. Both molecules show well-resolved redox waves of Fe(II)/Fe(III). $Fe(tpySCH_3)_2(OTF)_2$ shows anodic peak potential, E_{pa}, at 0.90 V and cathodic peak potential, E_{pc}, at 0.82 V, and ΔE_p is 74 mV. $Fe(tpySCH_2\text{-}pyr)_2(OTF)_2$ shows E_{pa} = 0.93 V, E_{pc} = 0.89 V and and ΔE_p = 44 mV, and a large, irreversible anodic peak beyond 1.1 V is also observed. Voltammograms of $Fe(tpySCH_3)_2(OTF)_2$ shows a ΔE_p of 74 mV (> 59 mV), which is consistent theoretically with a diffusing compound and with modest electron transfer kinetics. On the other hand, $Fe(tpySCH_2\text{-}pyr)_2(OTF)_2$ shows a ΔE_p of 44 mV (< 59 mV) – theoretically impossible for a purely diffusing compound, hence it is concluded that $Fe(tpySCH_2\text{-}pyr)_2(OTF)_2$ must be surface-bound,

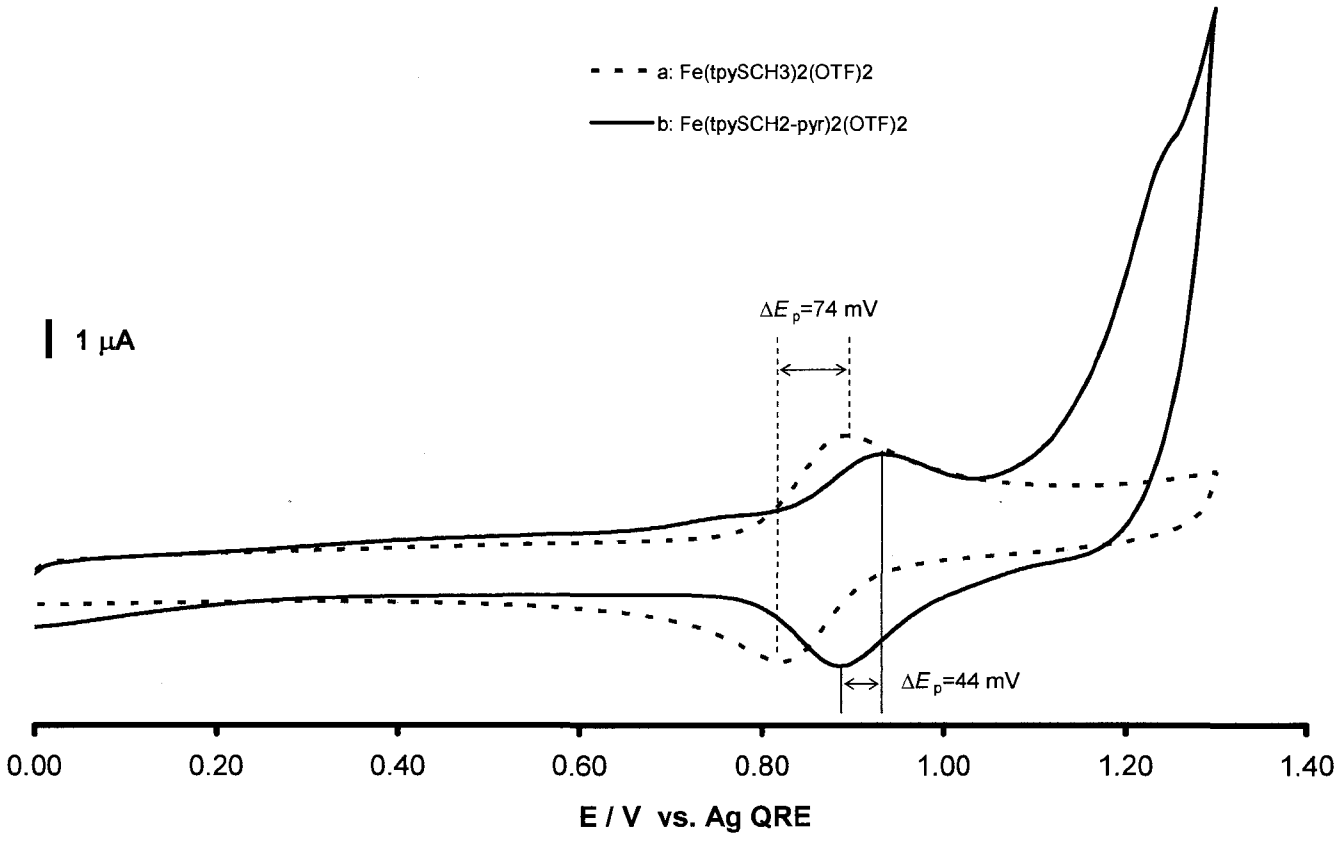

Figure 8. Comparison of the cyclic voltammograms of (a) $Fe(tpySCH_3)_2(OTF)_2$ and (b) $Fe(tpySCH_2\text{-}pyr)_2(OTF)_2$ at a GC electrode scanned 100 mV $s.^{-1}$

and clearly this behavior is due to the pyrenyl groups. The oxidation wave beyond 1.1 V that appears in the voltammogram of $Fe(tpySCH_2\text{-}pyr)_2(OTF)_2$ but not in $Fe(tpySCH_3)_2(OTF)_2$ must also correspond to the oxidation of pyrenyl groups.

3.2.1. Scan Rate Studies

Scan rate studies of $Fe(tpySCH_3)_2(OTF)_2$ and $Fe(tpySCH_2\text{-}pyr)_2(OTF)_2$ were carried out to study the scan rate dependence of the peak current of molecules and to support the previous observations. Both $Fe(tpySCH_3)_2(OTF)_2$ and $Fe(tpySCH_2\text{-}pyr)_2(OTF)_2$ solution were scanned with 20, 50, 100, 200, 500 and 1000 mV s^{-1} scan rates at a GC electrode. The solution in the cell that contains the analyte was then replaced with a fresh electrolyte solution without cleaning the electrode and another series of CVs were scanned under the same setting and scan rates. Figures 9 to 11 are voltammograms for solutions of $Fe(tpySCH_3)_2(OTF)_2$ (Figure 9), $Fe(tpySCH_2\text{-}pyr)_2(OTF)_2$ (Figure 10), and Figure 11 is a continuation of Figure 10 experiments but following exchange with fresh electrolyte. It is noteworthy that only a small decrease in anodic peak current, i_{pa}, took place following the exchange of the $Fe(tpySCH_2\text{-}pyr)_2(OTF)_2$ solution. For example, at scan rate of 100 mV s^{-1}, the peak current was 4.34 μA before and 3.92 μA after the exchange, so the pyrenyl complex is clearly retained on the GC electrode.

The plots of i_{pa} vs. sweep rate for the above three experiments are shown in Figure 12. As previously, non-Faradaic currents were subtracted. The equation $i_{pa} = 0.36\upsilon^{0.48}$ was obtained for $Fe(tpySCH_3)_2(OTF)_2$, which shows that the peak current of $Fe(tpySCH_3)_2(OTF)_2$ is closely proportional to the square root of the sweep rate. This indicates that the electrode reaction of $Fe(tpySCH_3)_2(OTF)_2$ is a diffusion-controlled

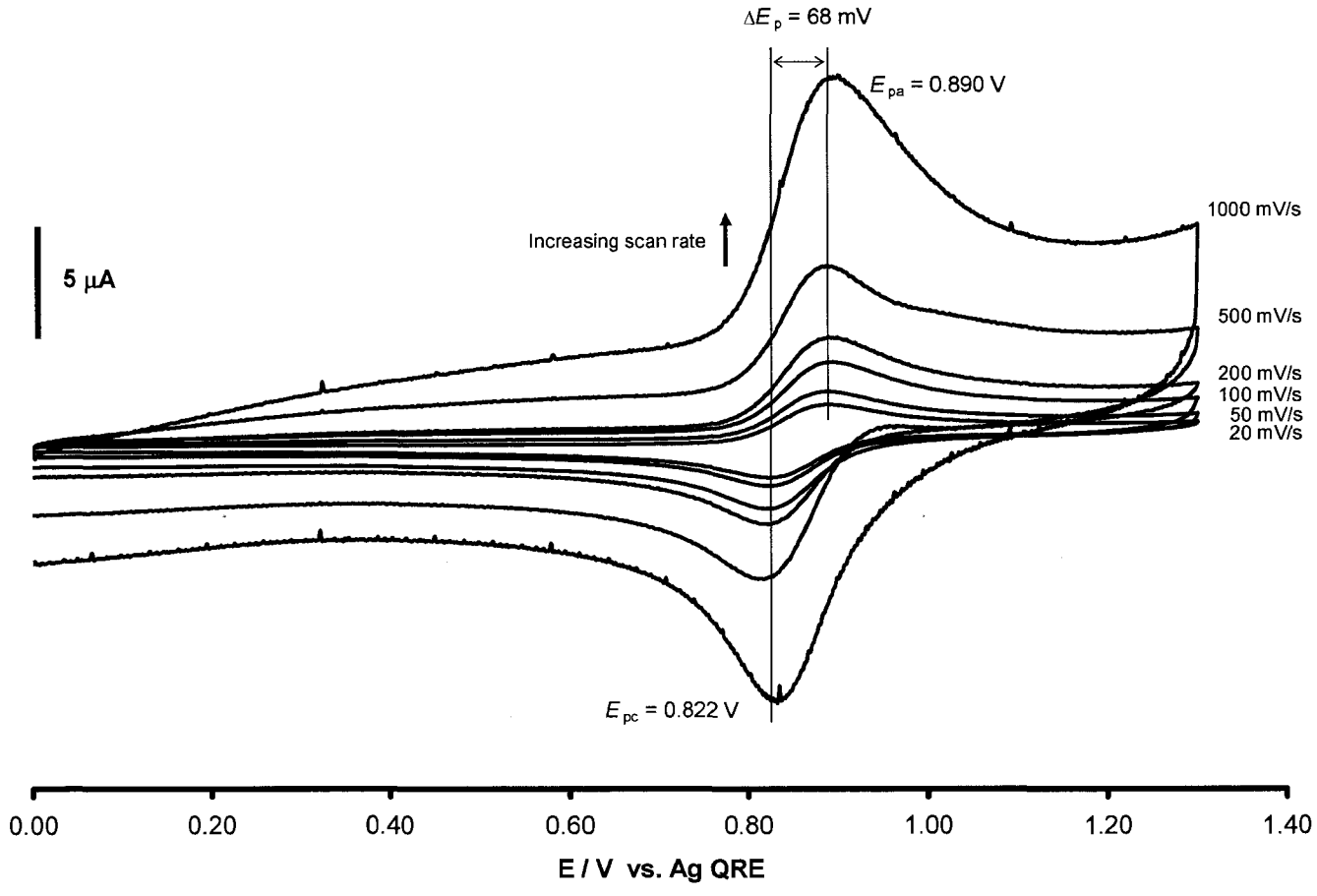

Figure 9. Cyclic voltammograms of $Fe(tpySCH_3)_2(OTF)_2$ at a GC electrode scanned from 0 to 1.3V with 20, 50, 100, 200, 500, 1000 mV s^{-1} scan rates.

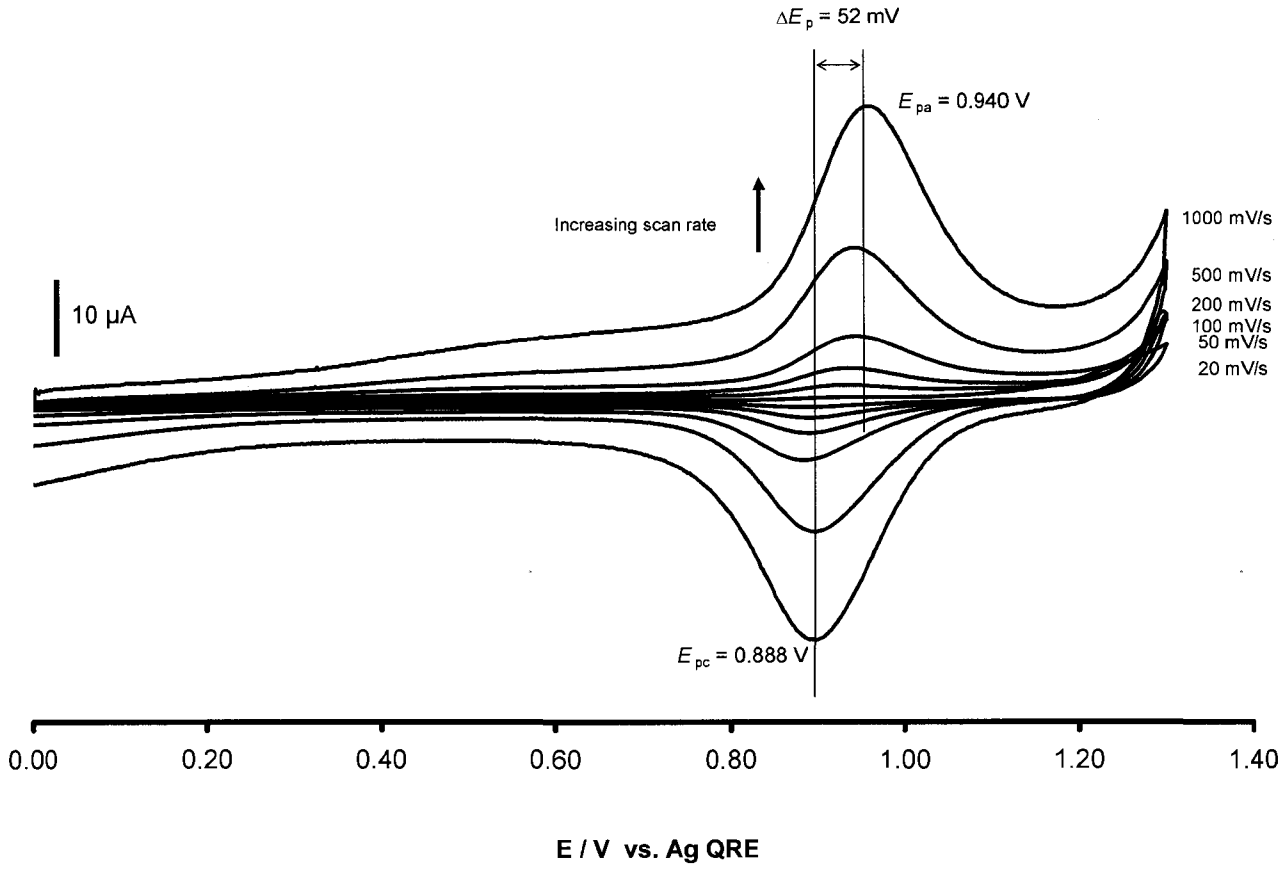

Figure 10. Cyclic voltammograms of $Fe(tpySCH_2\text{-}pyr)_2(OTF)_2$ at a GC electrode scanned from 0 to 1.3V with 20, 50, 100, 200, 500, 1000 mV s^{-1} scan rates.

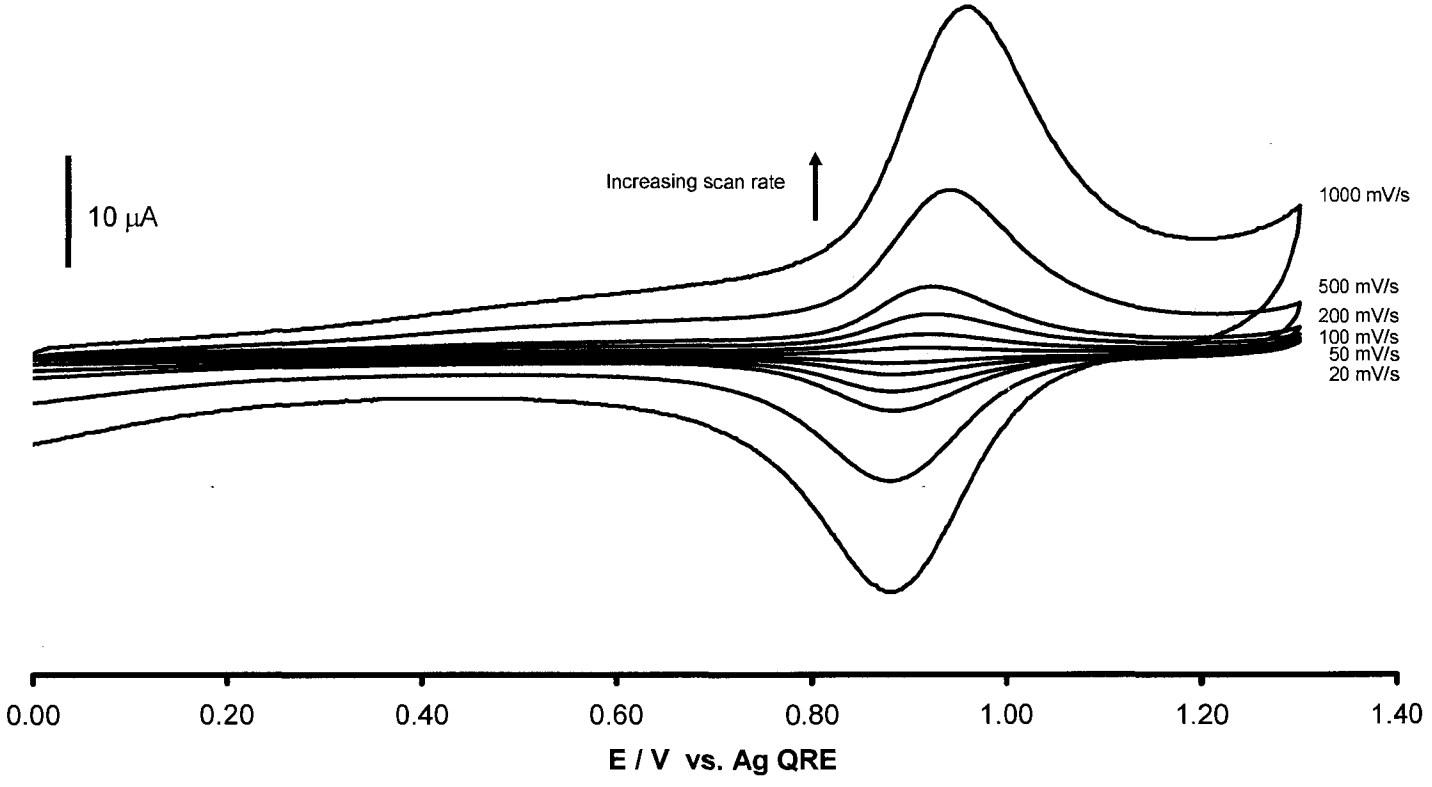

Figure 11. Cyclic voltammograms in the fresh electrolyte solution exchanged into the cell at a GC electrode scanned from 0 to 1.3V with 20, 50, 100, 200, 500, 1000 mV s^{-1} scan rates.

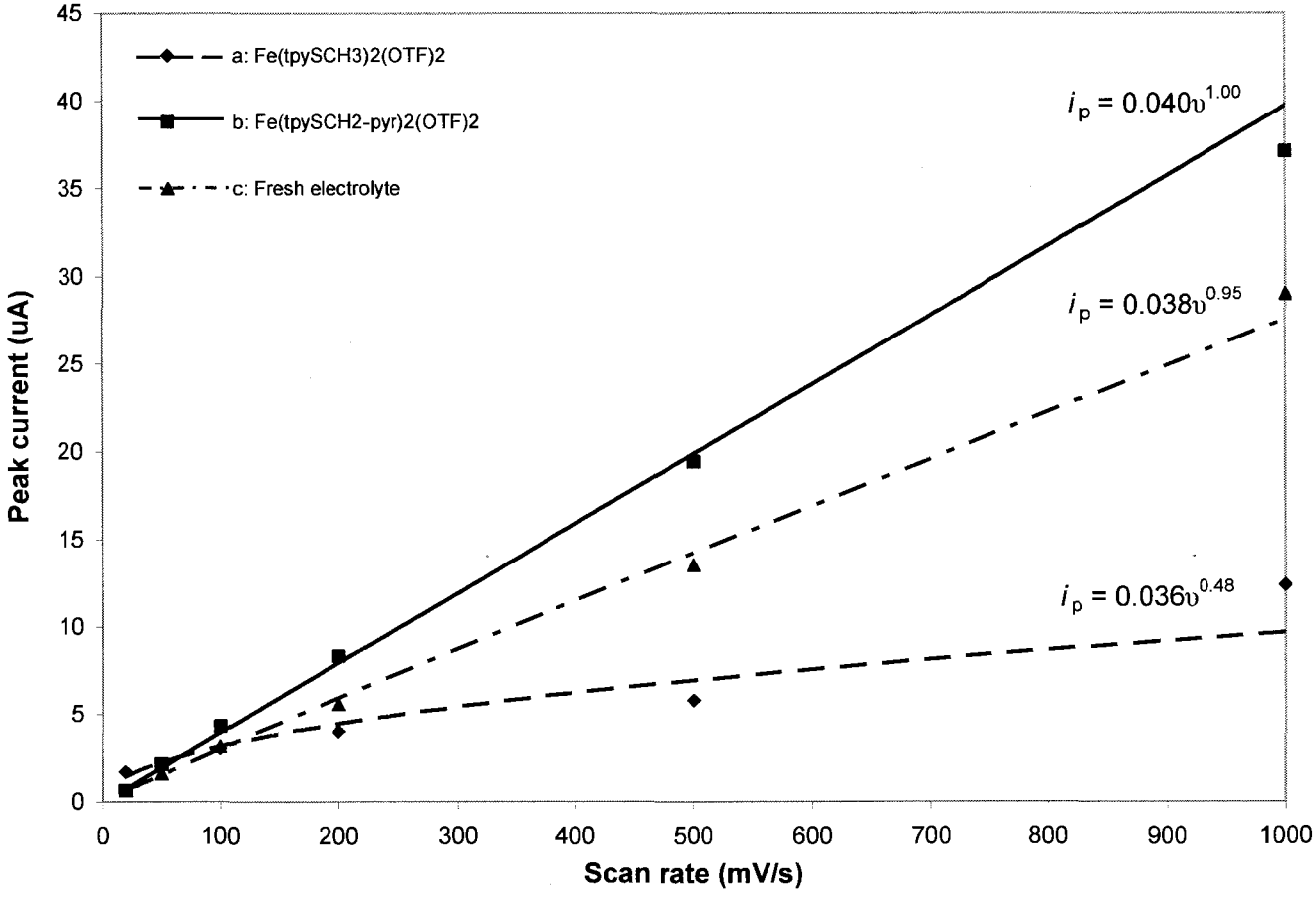

Figure 12. Sweep rate dependence of the peak current of at GC electrode of (a) $Fe(tpySCH_3)_2(OTF)_2$; (b) $Fe(tpySCH_2\text{-}pyr)_2(OTF)_2$; and (c) fresh electrolyte solution.

process at the GC electrode and $Fe(tpySCH_3)_2(OTF)_2$ molecules do not bind to the electrode surface.

The equation $i_{pa} = 0.040\upsilon^{1.00}$ was obtained for $Fe(tpySCH_2\text{-}pyr)_2(OTF)_2$, which shows that the peak current of $Fe(tpySCH_2\text{-}pyr)_2(OTF)_2$ has a linear proportionality to the sweep rate of the CV scans. The equation $i_{pa} = 0.038\upsilon^{0.95}$ was also obtained for the fresh electrolyte solution replacing the solution containing $Fe(tpySCH_2\text{-}pyr)_2(OTF)_2$. This is still close to a linear proportionality. According to the *Laviron equation*, for a surface-bound electrode reaction, there is a linear relationship between the peak current response and the sweep rates. Therefore, $Fe(tpySCH_2\text{-}pyr)_2(OTF)_2$ exhibits a surface-bound property at the GC electrode. The results of scan rate studies supported the observation of earlier CV experiments. Since $Fe(tpySCH_3)_2(OTF)_2$ and $Fe(tpySCH_2\text{-}pyr)_2(OTF)_2$ are molecules of similar structure except for the pyrenyl group on each terpyridine of $Fe(tpySCH_2\text{-}pyr)_2(OTF)_2$, it suggests that $Fe(tpySCH_2\text{-}pyr)_2(OTF)_2$ exhibits a surface-bound electrode reaction and binds to the electrode surface through the pyrenyl groups.

3.3. Time and Sweep Number Dependence of Signal for 50 μM $Fe(tpySCH_2\text{-}pyr)_2(OTF)_2$ at GC Electrodes

A series of CV scans of an electrolyte containing 50 μM $Fe(tpySCH_2\text{-}pyr)_2(OTF)_2$ were carried out at a GC electrode, and the voltammograms are shown in Figure 13. The CVs were run every 10 minutes from 0 to 1.3V at a scan rate of 100 mV s^{-1} with the analyte in solution. The peak splitting for this set of experiments remained roughly constant at 41 mV. Figure 14a is a plot of anodic peak current versus scan number and

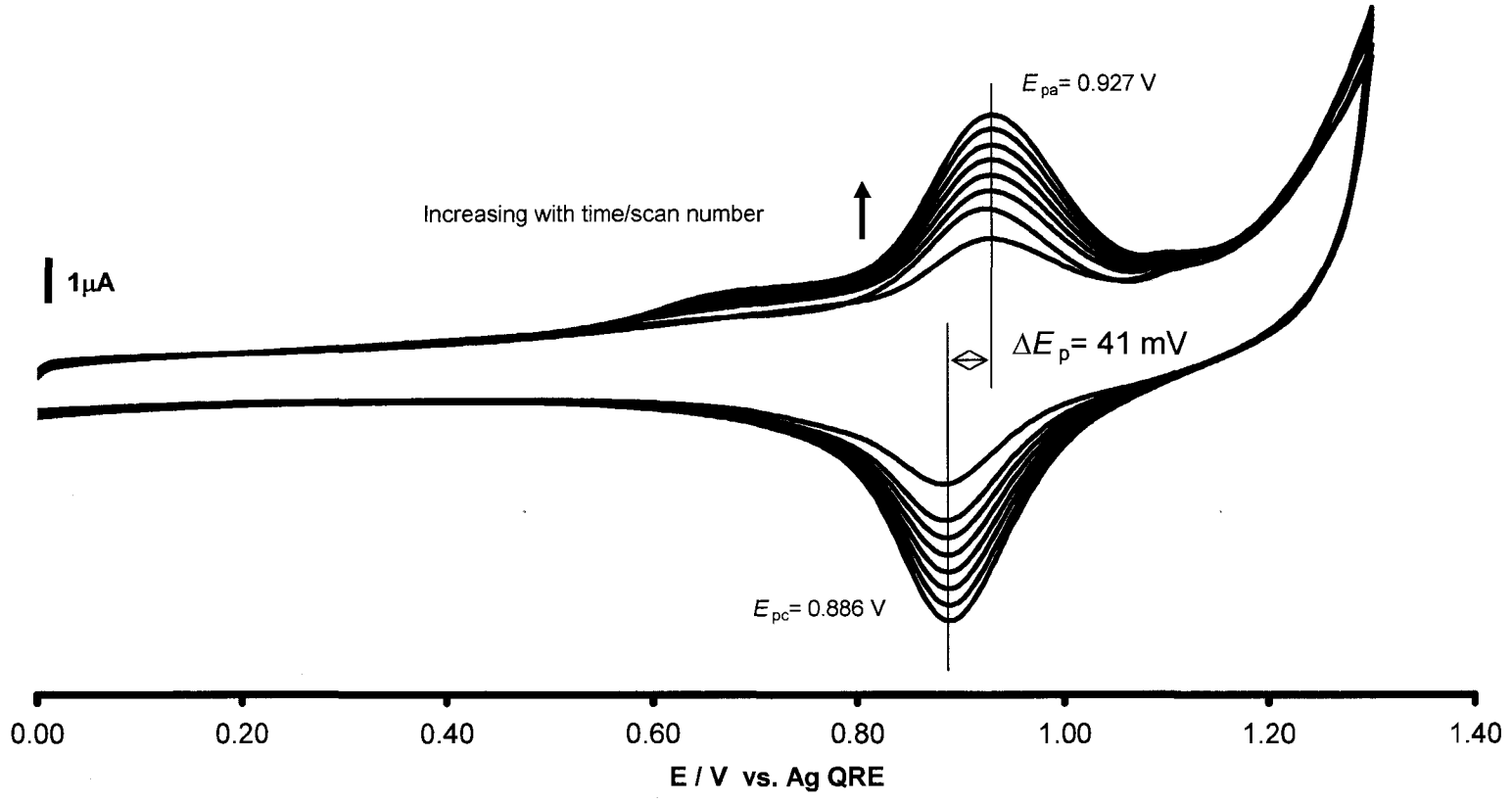

Figure 13. Sequent CVs of 50 μM $Fe(tpySCH_2\text{-}pyr)_2(OTF)_2$ at a GC electrode scanned 100 mV s^{-1} every 10 minutes from 0 to 1.3 V.

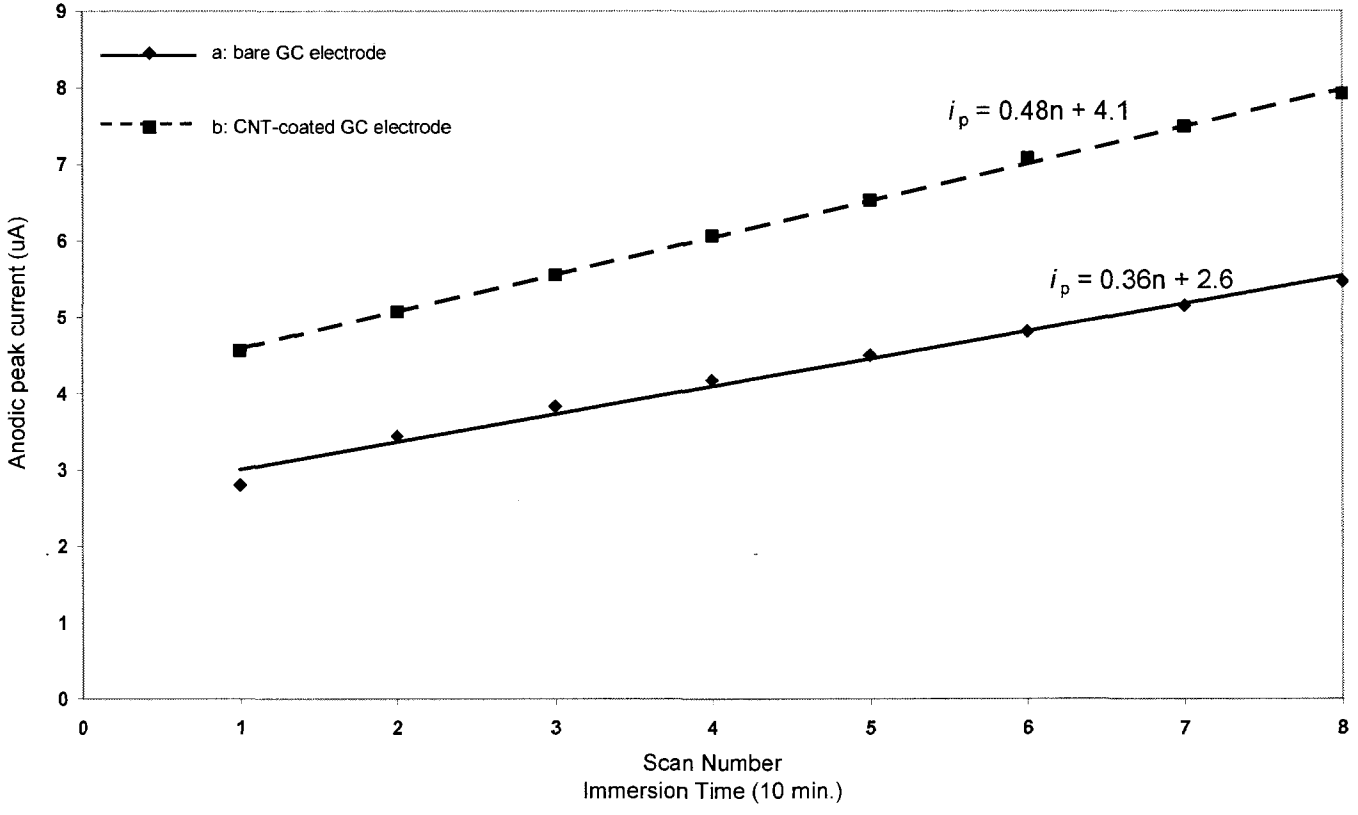

Figure 14. i_{pa} of 50 μM $Fe(tpySCH_2\text{-}pyr)_2(OTF)_2$ versus CV scan number and immersion time at (a) a bare GC and (b) the CNT-coated GC electrode.

immersion time, which shows that the peak current response increases linearly with immersion time or number of CV scans.

After a series of CVs were done with the analyte in the cell, a clean electrolyte solution was exchanged into the cell without cleaning the surface of GC electrode. Figure 15 is a series of voltammograms in which CVs were carried out every 10 minutes with the fresh electrolyte at the GC electrode. This series of CV scans were done under the same setting as the previous experiments using IP = 0, V1 = 1.3 V, V2 = 0 and scan rate of 100 mV $s.^{-1}$ In this series of voltammograms, $E_{pa} = 0.942$ V, $E_{pc} = 0.904$ V and $\Delta E_p = 38$ mV. The peak current responses remain about 4.5 μA after the analyte solution was replaced and stay high for a period of time. This suggests that the molecules of $Fe(tpySCH_2\text{-}pyr)_2(OTF)_2$ stay on the surface of electrode after the analyte solution in the cell has been removed.

3.3.1. Adsorbate Coverage and Molecular Layers

The integral and surface coverage of 50 μM $Fe(tpySCH_2\text{-}pyr)_2(OTF)_2$ on GC electrode were calculated using home built software. The model coverage of a monolayer is calculated as 1.7 nmol cm^{-2} by estimating that each $Fe(tpySCH_2\text{-}pyr)_2(OTF)_2$ molecule has a surface area of 1 $nm.^2$ The number of molecular layers is calculated by dividing the surface coverage by the model monolayer coverage. Table 1 lists the calculated integral, surface coverage and numbers of molecular layers formed on the electrode surface. The results show that 50 μM $Fe(tpySCH_2\text{-}pyr)_2(OTF)_2$ forms molecular multilayers on the GC electrode surface and the surface coverage and number

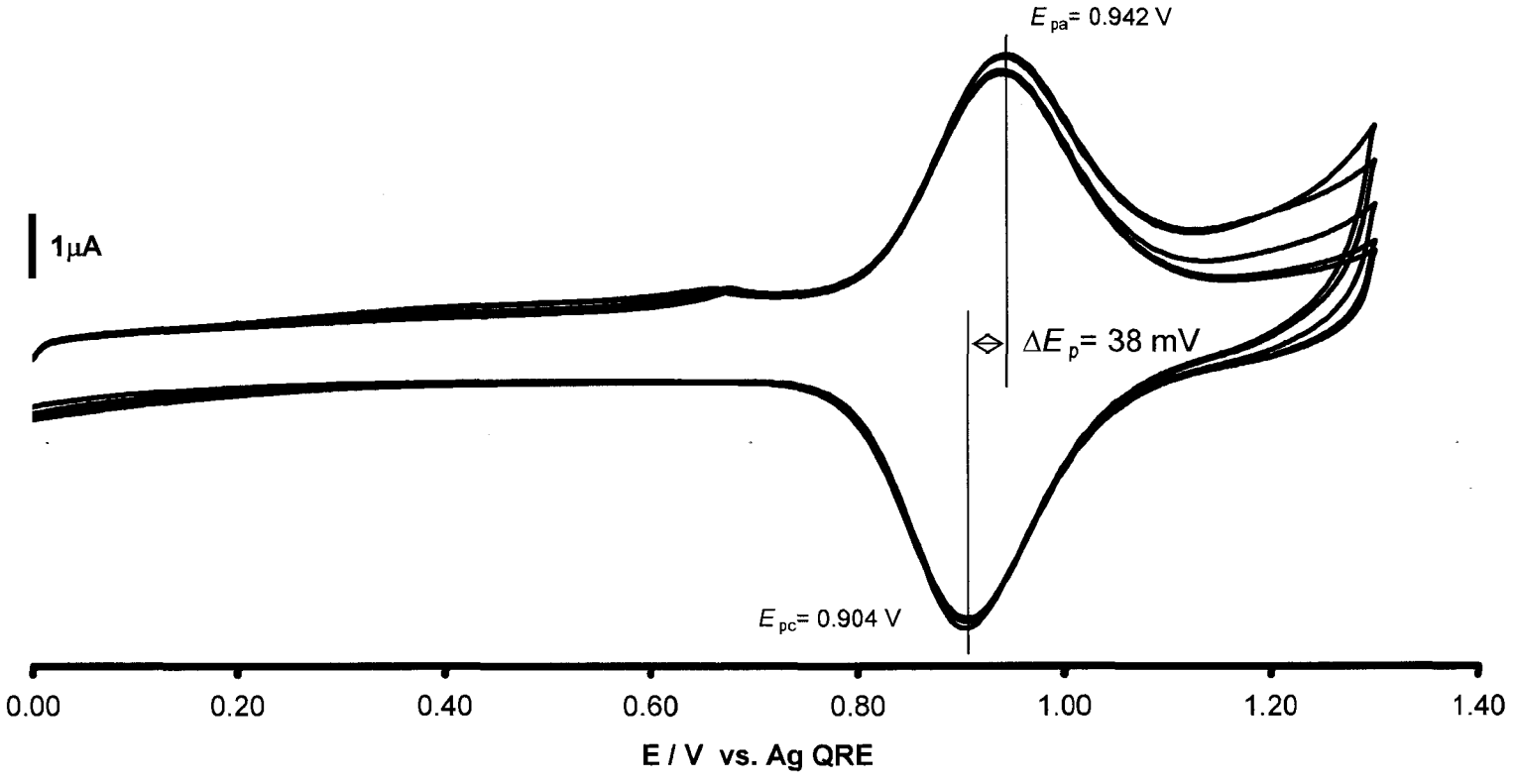

Figure 15. Cyclic voltammograms after the fresh electrolyte solution was exchanged into the cell at a GC electrode scanned 100 mV s^{-1} every 10 minutes.

Table 1. Integral, surface coverage and number of molecular layers of 50 μM Fe(tpySCH2-pyr)2(OTF)2 on a GC electrode with different scan number and immersion time. To calculate the number of molecular layers, the surface area of the molecule is estimated as 1 nm^2/molecule.

Scan Number	**Immersion Time (min)**	**Integral (μC)**	**Surface Coverage (nmol cm^{-2})**	**Number of Molecular Layers**
1	10	0.14	0.46	$2._8$
2	20	0.24	0.79	$4._7$
3	30	0.26	0.85	$5._1$
4	40	0.29	0.96	$5._8$
5	50	0.33	1.08	$6._5$
6	60	0.36	1.19	$7._2$
7	70	0.40	1.34	$8._0$
8	80	0.44	1.44	$8._7$

of molecular layers of $Fe(tpySCH_2\text{-}pyr)_2(OTF)_2$ increase with increasing number of CV scans or immersion time.

3.3.2. Effect of CV Scanning on $Fe(tpySCH_2\text{-}pyr)_2(OTF)_2$ Film Growth

As shown in Figures 13 and Table 1, the peaks of $Fe(tpySCH_2\text{-}pyr)_2(OTF)_2$ keep growing with repeating CV scanning every 10 minutes and molecular multilayers were formed on the electrode surface. A set of experiments were carried out to study the relationship between CV scanning, immersion time and the growth of molecular layers on the electrode by immersing two GC electrodes in 50 μM of $Fe(tpySCH_2\text{-}pyr)_2(OTF)_2$. The first GC electrode was immersed in 50 μM of $Fe(tpySCH_2\text{-}pyr)_2(OTF)_2$ and scanned repeatedly every minute for 60 minutes. The second GC electrode was scanned once after immersing in 50 μM of $Fe(tpySCH_2\text{-}pyr)_2(OTF)_2$ and then again after 60 minutes. The experiments were done by setting the program to IP = 0, V1 = 1.3 V, V2 = 0 and scan rate of 100 mV $s.^{-1}$ The resulting voltammograms are shown in Figure 16 and the integral and surface coverage are listed in Table 2.

The results show that the current response of the repeating one-minute scan 61 with immersion time of 60 minutes is much higher than that of scan 2 with the same immersion time. The peak current response of CV scan 2 with immersion time of 60 minutes is 2.29 μA, which is only slightly higher than the current response of 2.16 μA of the repeating one-minute scan 2 with immersion time of 1 minute. This suggests that CV scanning greatly affects the growth of $Fe(tpySCH_2\text{-}pyr)_2(OTF)_2$ on the surface of electrode and electropolymerization of pyrenyl groups of $Fe(tpySCH_2\text{-}pyr)_2(OTF)_2$ is implied.[24] With increasing numbers of CV scan, the numbers of molecular layers

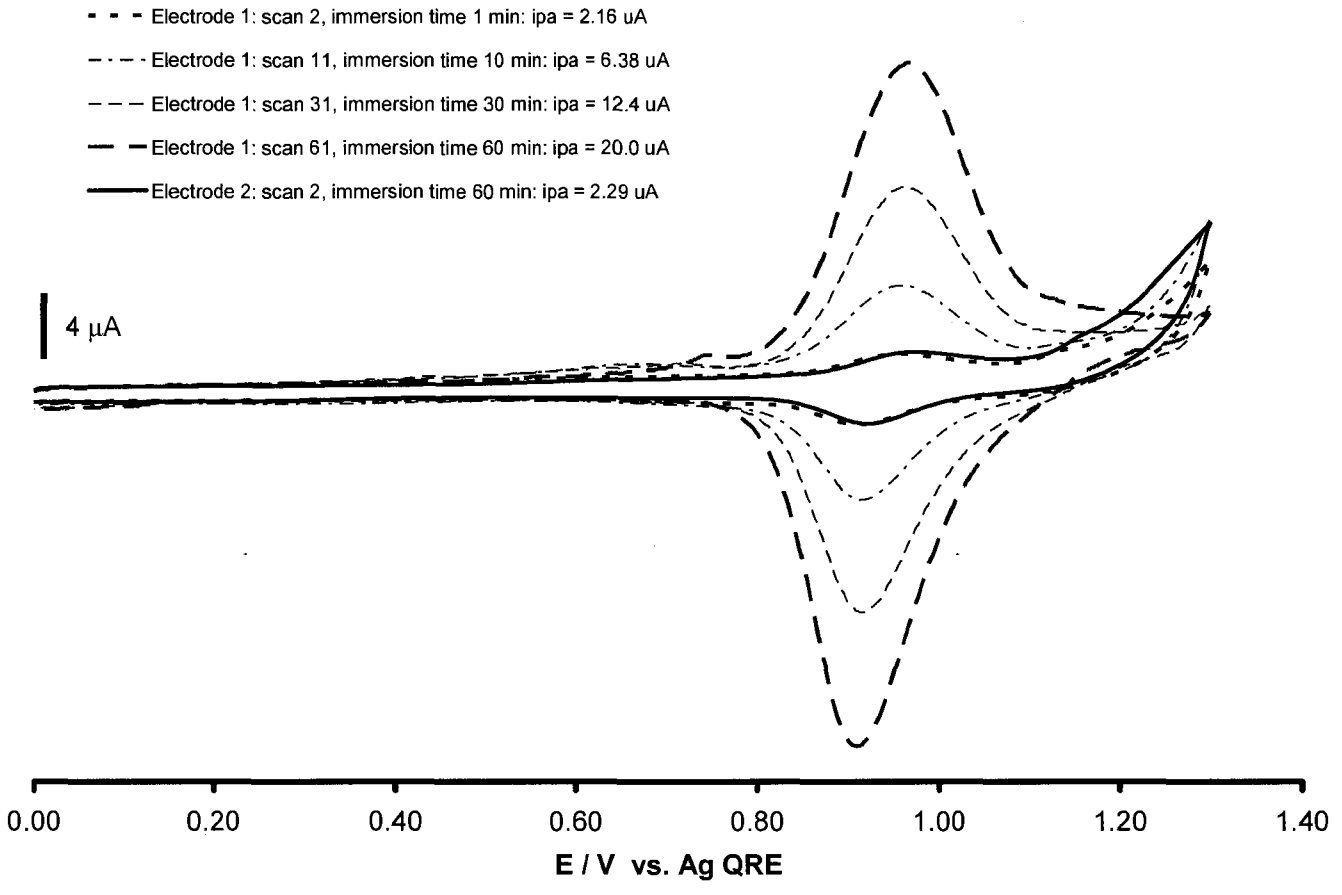

Figure 16. Effect of CV scanning on $Fe(tpySCH_2\text{-}pyr)_2(OTF)_2$ film growth. Two GC electrodes were immersed in 50 μM $Fe(tpySCH_2\text{-}pyr)_2(OTF)_2$ solution. Electrode 1 was scanned repeatedly every minute for 60 minutes. Electrode 2 was scanned once and then again after 60 minutes. Scan rate was 100 mV $s.^{-1}$

Table 2. Integral and surface coverage of two GC electrodes immersed in 50 μM $Fe(tpySCH_2\text{-}pyr)_2(OTF)_2$ with different immersion time and scanned with different number of CV scans. The first GC electrode was immersed in $Fe(tpySCH_2\text{-}pyr)_2(OTF)_2$ and scanned repeatedly every minute for 60 minutes. The second GC electrode was scanned once and then again after 60 minutes. To calculate the number of molecular layers, the surface area of the molecule is estimated as 1 nm^2/molecule.

Scan Number	**Immersion Time (min)**	**Integral (μC)**	**Surface Coverage (nmol cm^{-2})**	**Number of Molecular Layers**	**Electrode**
2	60	0.098	0.32	$1._9$	2
2	1	0.094	0.31	$1._9$	1
11	10	0.59	1.9	$11._4$	
21	20	1.0	3.4	$20._5$	
31	30	1.4	4.6	$27._7$	
41	40	1.8	5.9	$35._5$	
51	50	2.2	7.2	$43._4$	
61	60	2.4	8.0	$48._2$	

growing on the electrode surface also increase. It was observed that $Fe(tpySCH_2\text{-}pyr)_2(OTF)_2$ can form up to 50 molecular layers after 60 CV scans.

3.3.3. Physisorption of Pyrenyl Groups of $Fe(tpySCH_2\text{-}pyr)_2(OTF)_2$ onto GC Surface

A "zero-scan" experiment was carried out to investigate if $Fe(tpySCH_2\text{-}pyr)_2(OTF)_2$ would physisorb on the surface of electrode without polymer formation induced by CV scanning. In this experiment, the polished GC electrode was first immersed in 50 μM of $Fe(tpySCH_2\text{-}pyr)_2(OTF)_2$ solution for 5 minutes *without scanning,* rinsed with solvent and then scanned in fresh electrolyte using IP = 0, V1 = 1.05 V, V2 = 0. The switching potential, V1, was set to 1.05 V which is before the oxidation of pyrene takes place. The resulting voltammogram shows no distinct peak. Another experiment was then carried out by immersing the polished GC electrode in 50 μM $Fe(tpySCH_2\text{-}pyr)_2(OTF)_2$ solution for 20 minutes, rinsing with solvent and run a CV in fresh electrolyte to see if longer immersion time would have any effect on the CV results. However, immersing the electrode in 50 μM solution longer did not change the experimental results. The resulting voltammogram still shows no distinct peak. The polished GC electrode was then immersed in 500 μM $Fe(tpySCH_2\text{-}pyr)_2(OTF)_2$ solution for 10 minutes to see if immersing the electrode in solution with a larger concentration would produce different CV results. The CV was scanned under the same potential settings as the previous experiment and run in fresh electrolyte. The resulting voltammograms and calculated integral and surface coverage are shown in Figure 17 and Table 3. The CV scans by the

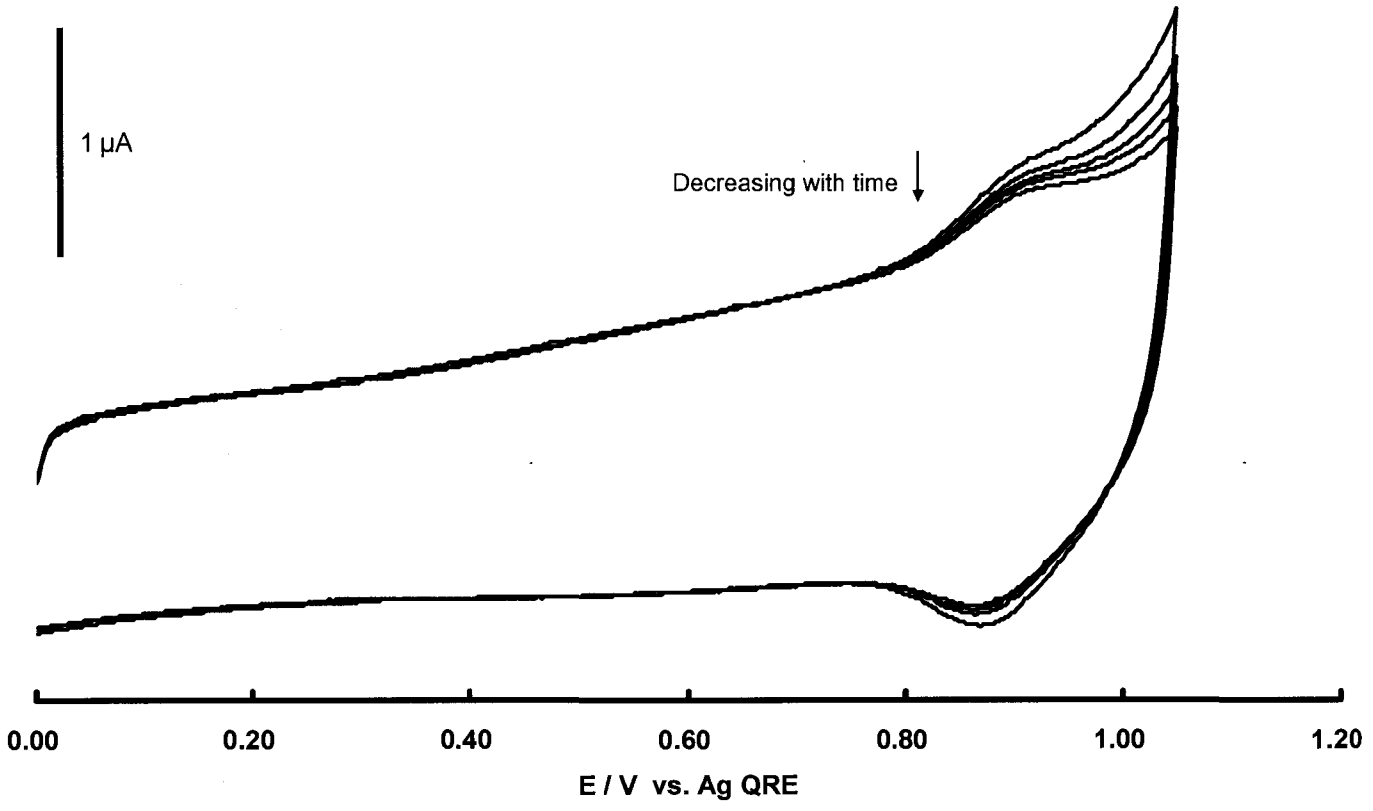

Figure 17. Cyclic voltammograms of sequent CV scans at the GC electrode immersed in 500 µM $Fe(tpySCH_2\text{-}pyr)_2(OTF)_2$ solution for 10 minutes and rinsed with solvent, and CV scans were run in fresh electrolyte.

Table 3. Integral and surface coverage of $Fe(tpySCH_2\text{-}pyr)_2(OTF)_2$ on a GC electrode immersed in 500 μM solution for 10 minutes and rinsed with solvent and run CV scan several times in clean electrolyte. Surface area of the molecule is estimated as 1 nm^2/molecule.

Scan Number	**Integral (μC)**	**Surface Coverage (nmol cm^{-2})**	**Number of Molecular Layers**
1	0.032	0.11	0.6_4
2	0.030	0.099	0.6_0
3	0.029	0.096	0.5_8
4	0.028	0.092	0.5_6
5	0.027	0.089	0.5_4

GC electrode immersed in 500 μM $Fe(tpySCH_2\text{-}pyr)_2(OTF)_2$ solution for 10 minutes and rinsed with solvent give redox waves with surface coverage of 0.107 nmol cm^{-2} with a molecular submonolayer on the surface of electrode. Several sequent CV scans also show the same results with a little smaller molecular coverage. This suggests that the molecules would adsorb on the electrode surface without CV scanning after immersing the electrode in a solution with high enough concentration, and the molecules would gradually desorb away from the electrode surface after a period of time.

3.4. Comparison of a Bare GC and the CNT-coated GC Electrode

A set of experiments were carried out at a CNT-coated GC electrode in 50 μM $Fe(tpySCH_2\text{-}pyr)_2(OTF)_2$ solution and the results were compared with that of a bare GC to the CNT-coated electrode. Figure 18 shows the voltammograms of CVs scanned every 10 minutes by setting IP = 0, V1 = 1.3 V, V2 = 0 and scan rate of 100 mV s^{-1} with 50 μM $Fe(tpySCH_2\text{-}pyr)_2(OTF)_2$ in electrolyte. E_{pa} of $Fe(tpySCH_2\text{-}pyr)_2(OTF)_2$ at CNT coated GC electrode is 0.888 V, E_{pc} is 0.836 V and ΔE_p is 52 mV. The anodic peak current responses at the CNT-coated GC electrode were plotted versus scan numbers and immersion time and the plot is shown in Figure 14b. Similar to the result obtained from the experiments done at a bare GC electrode, the peak current response increases linearly with number of CV scans and molecular layers grow on both GC and CNT-coated GC electrodes.

However, with a CNT coating, the peak current responses at the CNT-coated electrode were observed to be higher than that at a bare GC electrode at each scan. Figure 19 shows a comparison between results observed under 100 mV s^{-1} scan rate at a

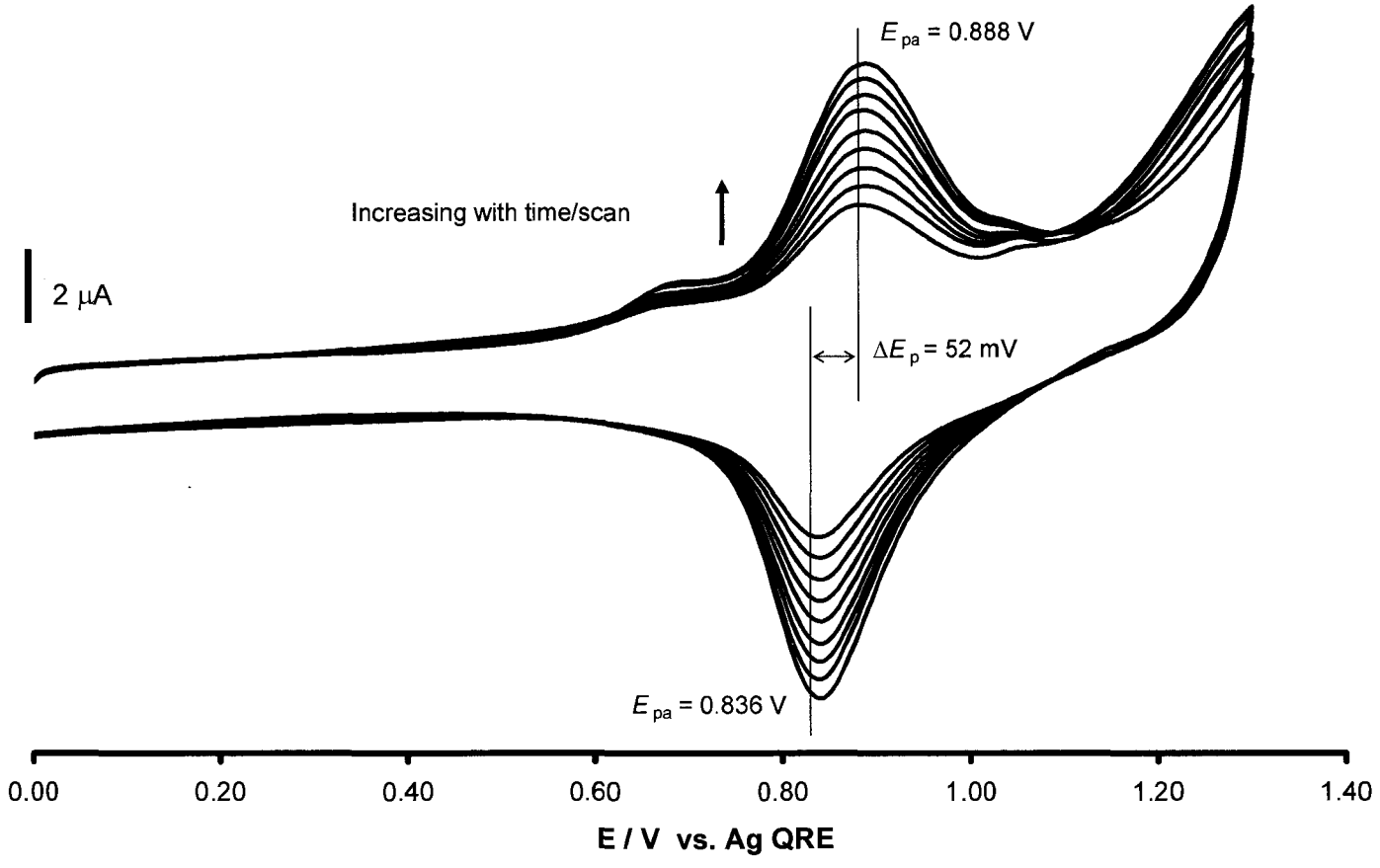

Figure 18. Cyclic voltammograms of sequent CV scans in 50 μM $Fe(tpySCH_2\text{-}pyr)_2(OTF)_2$ at a CNT-coated GC electrode scanned 100 mV s^{-1} from 0 to 1.3 V every 10 minutes.

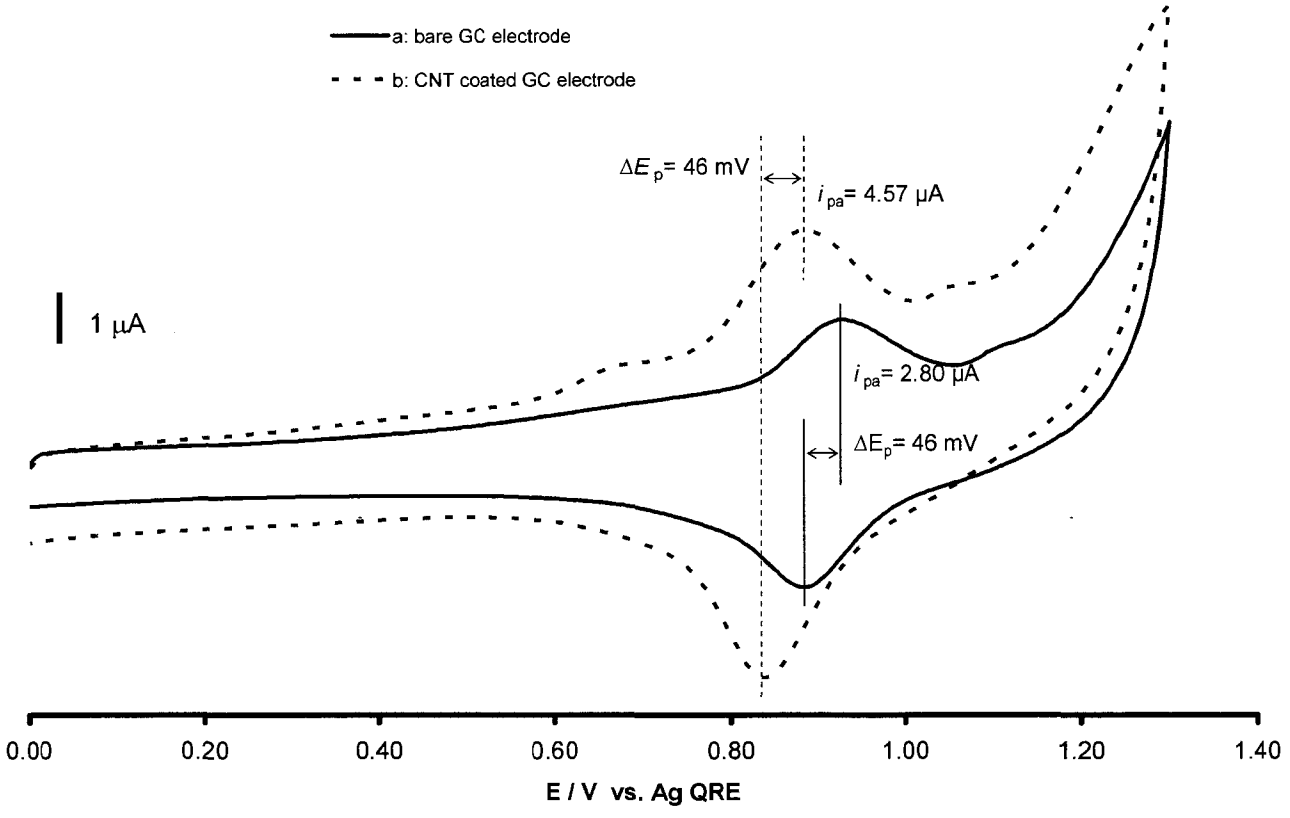

Figure 19. Comparison between the cyclic voltammograms of 50 μM $Fe(tpySCH_2\text{-}pyr)_2(OTF)_2$ at (a) a bare GC and (b) a CNT-coated GC electrode scanned 100 mV s^{-1} from 0 to 1.3 V.

bare GC and a CNT-coated GC electrode. With the concentration of $Fe(tpySCH_2\text{-}pyr)_2(OTF)_2$ controlled at 50 μM, at the bare GC electrode, i_{pa} is 2.80 μA, and at a CNT-coated GC electrode, i_{pa} increases to 4.57 μA. The coating of CNT films on the surface of a GC electrode can increase surface area and enhance the sensitivity of the electrode.

Figure 20 is a series of voltammograms of fresh electrolyte solution at the CNT-coated GC electrode. A 50 μM $Fe(tpySCH_2\text{-}pyr)_2(OTF)_2$ solution originally in the cell was replaced with fresh electrolyte without cleaning the surface of electrode in order to study the interaction between the electrode surface and the molecules. This series of CV scans were carried out under the same experimental conditions as the previous experiments setting IP = 0, V1 = 1.3 V, V2 = 0 and scan rate of 100 mV $s,^{-1}$ and CVs were scanned every 10 minutes. From the resulting voltammograms, E_{pa} = 0.944 V, E_{pc} = 0.894 V and ΔE_p = 50 mV. Figure 20 shows that with a total number of 7 scans, i_{pa} remains around 7.65 μA after the analyte solution has been removed. Compared to the value of i_{pa} = 4.5 μA at a bare GC electrode after the solution was replaced by a clean electrolyte, this also suggests that the molecules of $Fe(tpySCH_2\text{-}pyr)_2(OTF)_2$ stay on the surface of CNT-coated GC electrode and a high sensitivity of the CNT-coated GC electrode is retained after the analyte solution in the cell has been removed.

3.5. Spectroelectrochemistry

A spectroelectrochemical experiment was carried out using UV-Vis spectroscopy to study the extent of Fe(II)/Fe(III) oxidation. The analysis was done by coupling the electrochemical setup with to a UV-Vis spectrophotometer in order to monitor the change in absorbance responding to different applied voltages. Indium tin oxide (ITO) was used

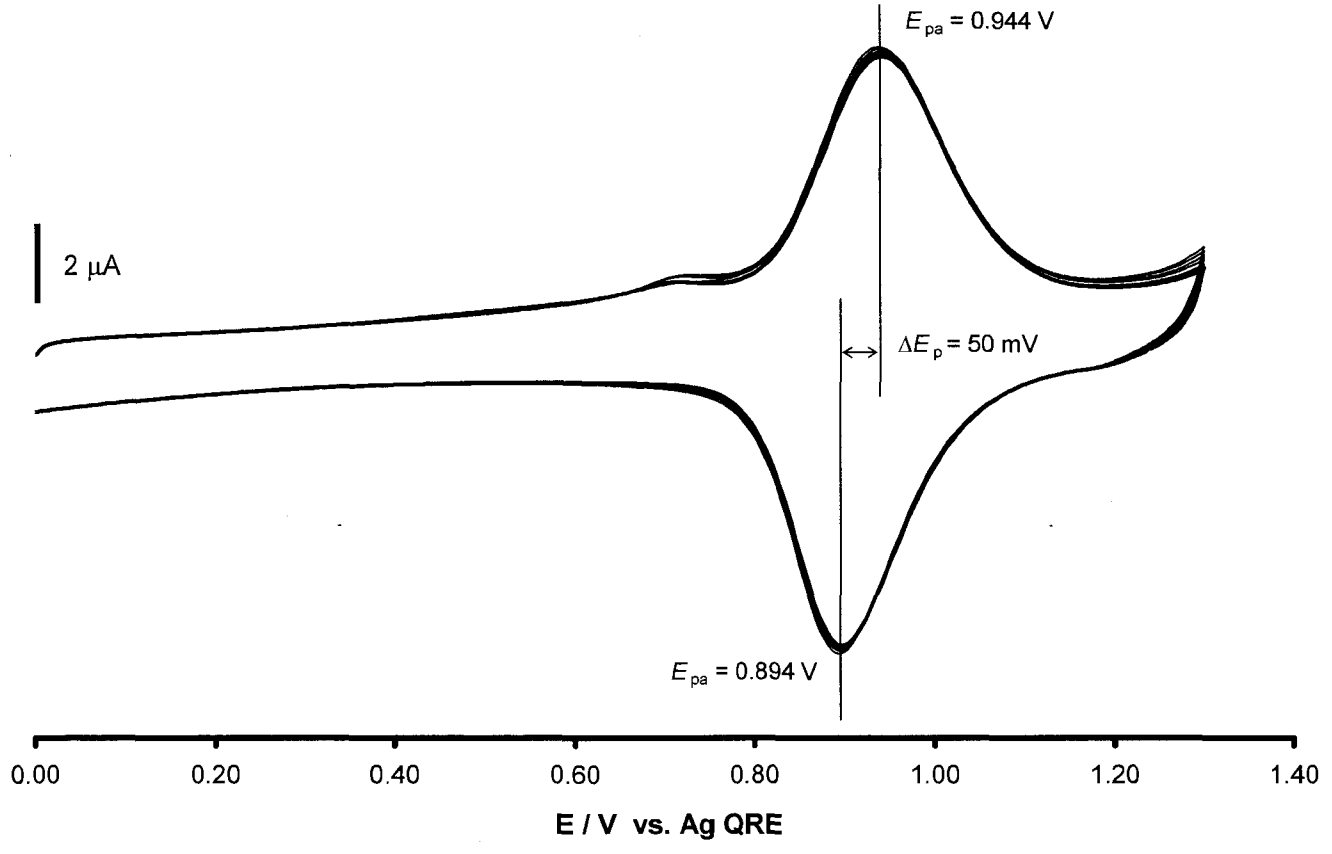

Figure 20. Cyclic voltammograms of sequent CV scans in the fresh electrolyte exchanged into the cell at a CNT-coated GC electrode scanned 100 mV s^{-1} every 10 minutes.

as the working electrode and a thin layer of $Fe(tpySCH_2\text{-}pyr)_2(OTF)_2$ was deposited onto the electrode surface by several consecutive CV scans from 0 to 1.3 V with solution in the cuvette. A fresh electrolyte was then exchanged into the cuvette to monitor the absorbance spectra from 300 to 800 nm with various voltages from 500 to 1300 mV applied. The resulting spectra are shown in Figure 21. Absorbance of the peak at 571 nm decreased with increasing potential applied, which corresponded to Fe(II)/Fe(III) oxidation. Two clear isosbestic points were observed at 474 and 642 nm.

The absorbances of the peak at 571 nm at different applied voltages were plotted against an ideal Nernstian response obtained from the *Nernst Equation*:[16]

$$E = E^0 + \frac{RT}{nF} \ln \frac{\Gamma_O}{\Gamma_R} \qquad (4)$$

The results are shown in Figure 22. The experimental results show a good fit to the ideal Nernstian response and reversbility of the reaction was implied. A small electroinactive region was also observed.

3.6. Au and CNT-coated Au Electrodes

The same sets of CV experiments were also carried out using Au as the working electrode. 50 μM $Fe(tpySCH_2\text{-}pyr)_2(OTF)_2$ was first analyzed at both Au and CNT-coated Au electrodes and the solution was replaced with fresh electrolyte afterward. Figure 23 shows a series of voltammograms of 50 μM $Fe(tpySCH_2\text{-}pyr)_2(OTF)_2$ scanned every 10 minutes, and Figure 24 shows the voltammograms of 50 μM $Fe(tpySCH_2\text{-}$

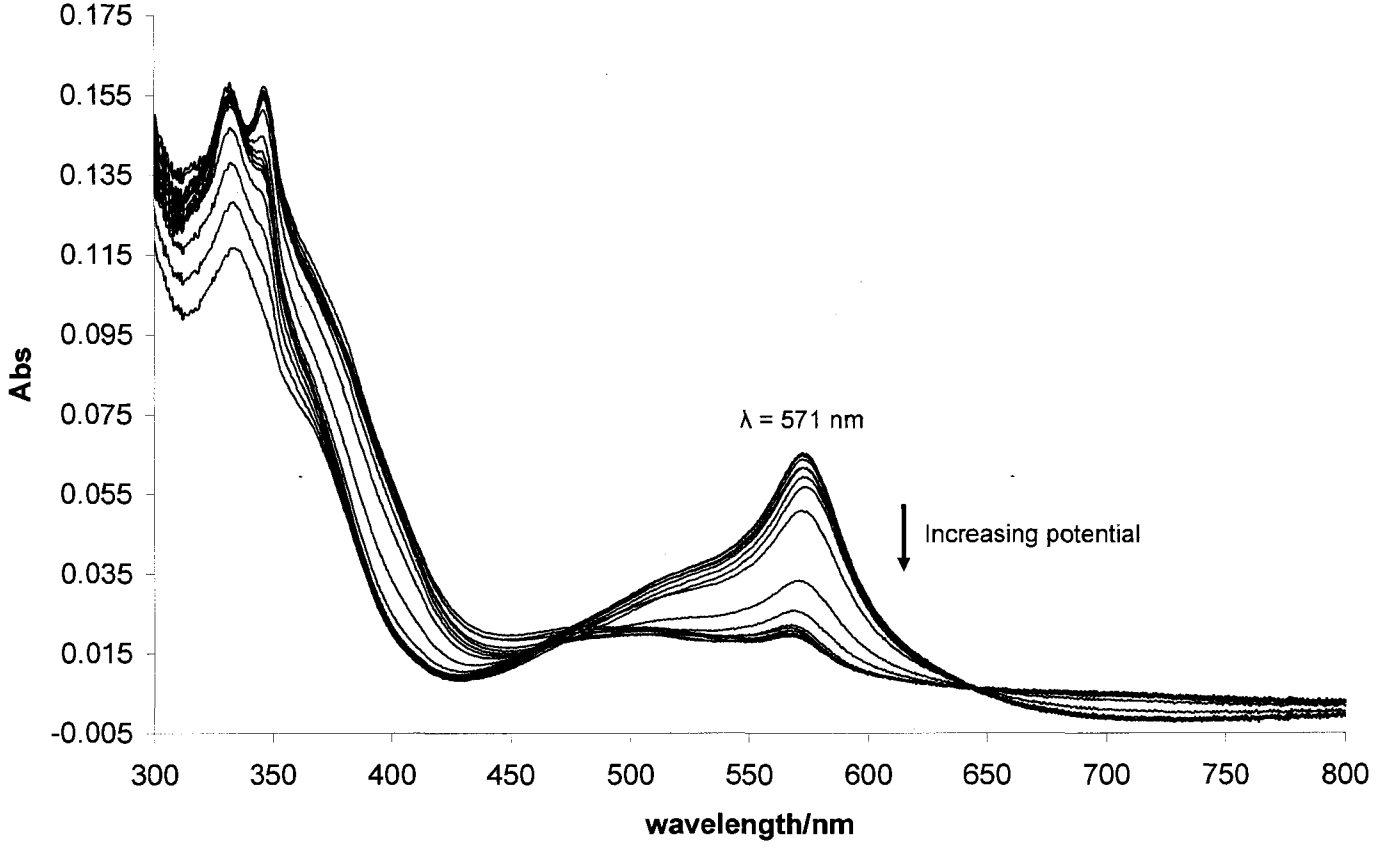

Figure 21. Spectroelectrochemical analysis with UV-Vis spectroscopy using ITO as working electrode. Voltages from 500 to 1300 mV were applied and the absorbance from 300 to 800 nm were measured.

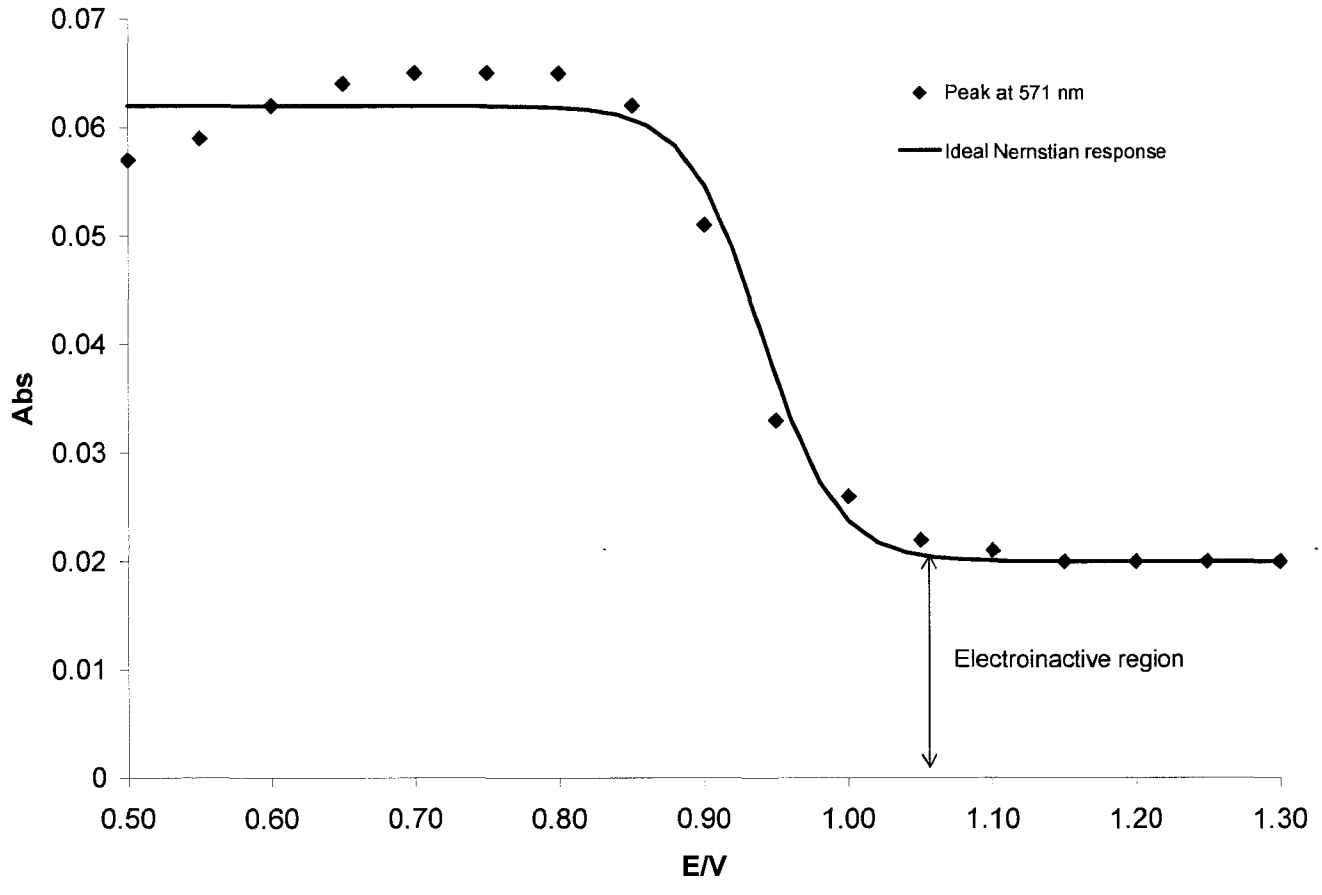

Figure 22. Plot of the spectroelectrochemical data. The absorbances of the peak at 571 nm at different applied voltages is plotted and compared to an ideal Nernstian response.

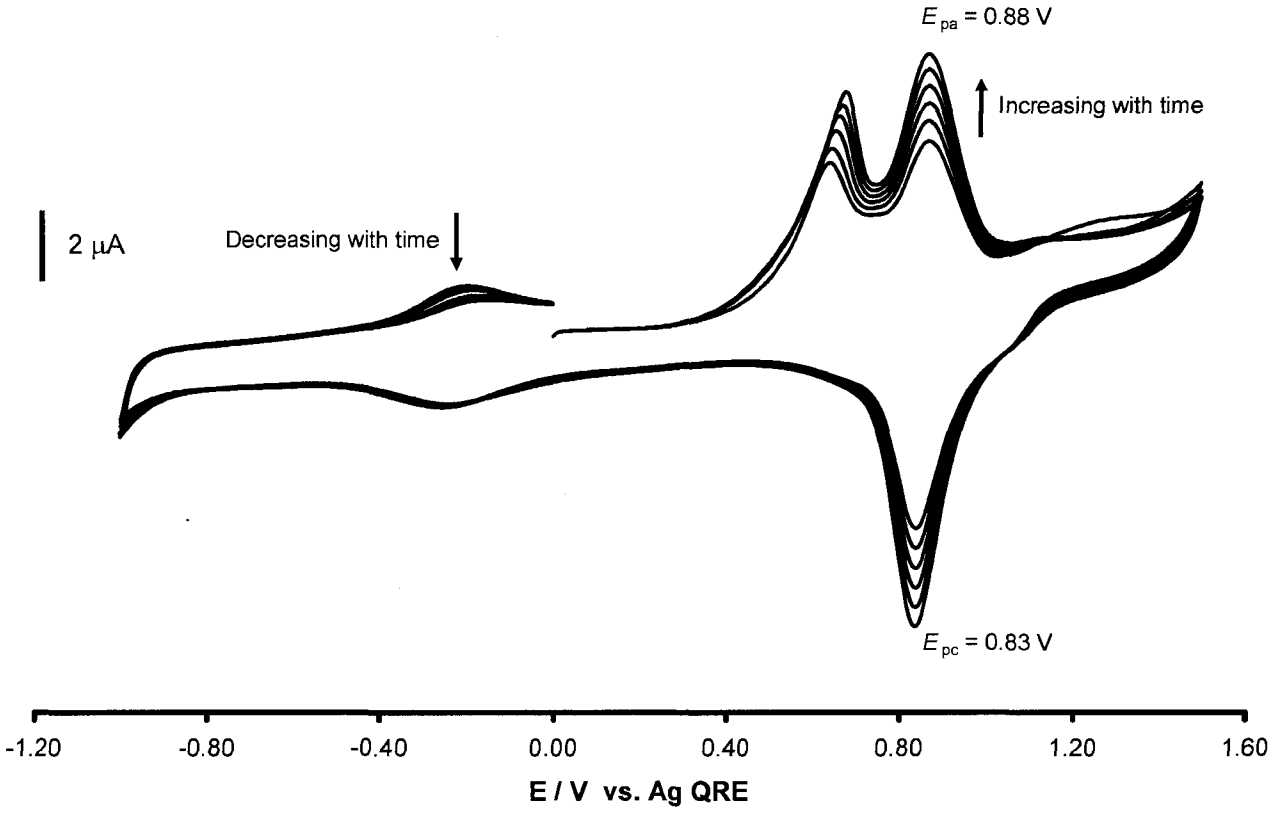

Figure 23. Cyclic voltammograms of 50 μM $Fe(tpySCH_2\text{-}pyr)_2(OTF)_2$ at a gold electrode scanned 100 mV s^{-1} from -1.0 to 1.5V every 10 minutes.

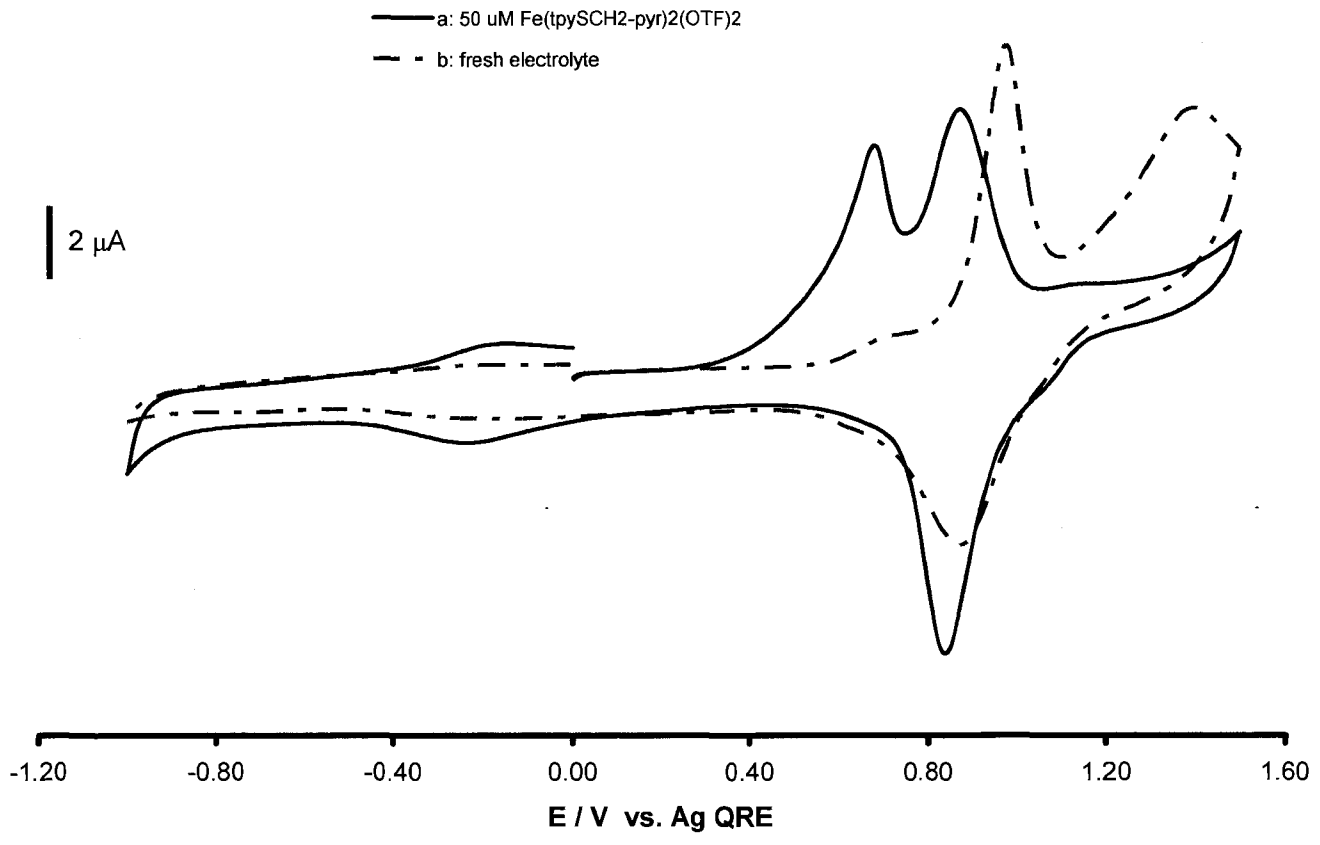

Figure 24. Comparison of the cyclic voltammograms of 50 µM $Fe(tpySCH_2\text{-}pyr)_2(OTF)_2$ in the cell and of the fresh electrolyte solution at a bare Au electrode scanned 100 mV s^{-1} from -1.0 to 1.5 V.

pyr)$_2$(OTF)$_2$ being replaced with fresh electrolyte solution at a bare Au electrode setting IP = 0, V1 = 1.5 V, V2 = -1 V and scan rate of 100 mV s.$^{-1}$ In Figure 23, the peak currents of anodic peaks at 0.67 V and 0.88 V and a cathodic peak at 0.83V increase with scan number and the current of the waves around -0.2 V decreases with scan number. After the analyte solution in the cell was replaced by a fresh electrolyte, only the redox waves shown around 1.0 V were retained (Figure 24). The retention of the redox waves shows that Fe(tpySCH$_2$-pyr)$_2$(OTF)$_2$ molecules stay on the Au electrode surface and are not washed away by replacing the solution in the cell.

Compared to the GC electrode, experiments done at an Au electrode exhibit more complicated results. The voltammograms of 50 μM Fe(tpySCH$_2$-pyr)$_2$(OTF)$_2$ in solution show a sharp anodic peak around 0.67 V increasing with scan number and waves around -0.2 V decreasing with scan number, but these two peaks are not seen in the voltammogram of the fresh electrolyte. These peaks may be related to the interaction between the sulfur and gold electrode. However, the explanations and actual causes of these peaks remain unclear.

The comparison between the voltammograms of 50 μM Fe(tpySCH$_2$-pyr)$_2$(OTF)$_2$ at a bare Au and a CNT-coated Au electrode is shown in Figure 25. The CVs were scanned under the same experimental conditions with a scan rate of 100 mV s,$^{-1}$ and the CV results show a higher current response at a CNT-coated Au electrode. This is consistent with the results obtained from the previous experiments done at a GC electrode. With a coating of CNT on the electrode surface, the surface area of the electrode and the resulting current response increase and the sensitivity of the electrode can be enhanced.

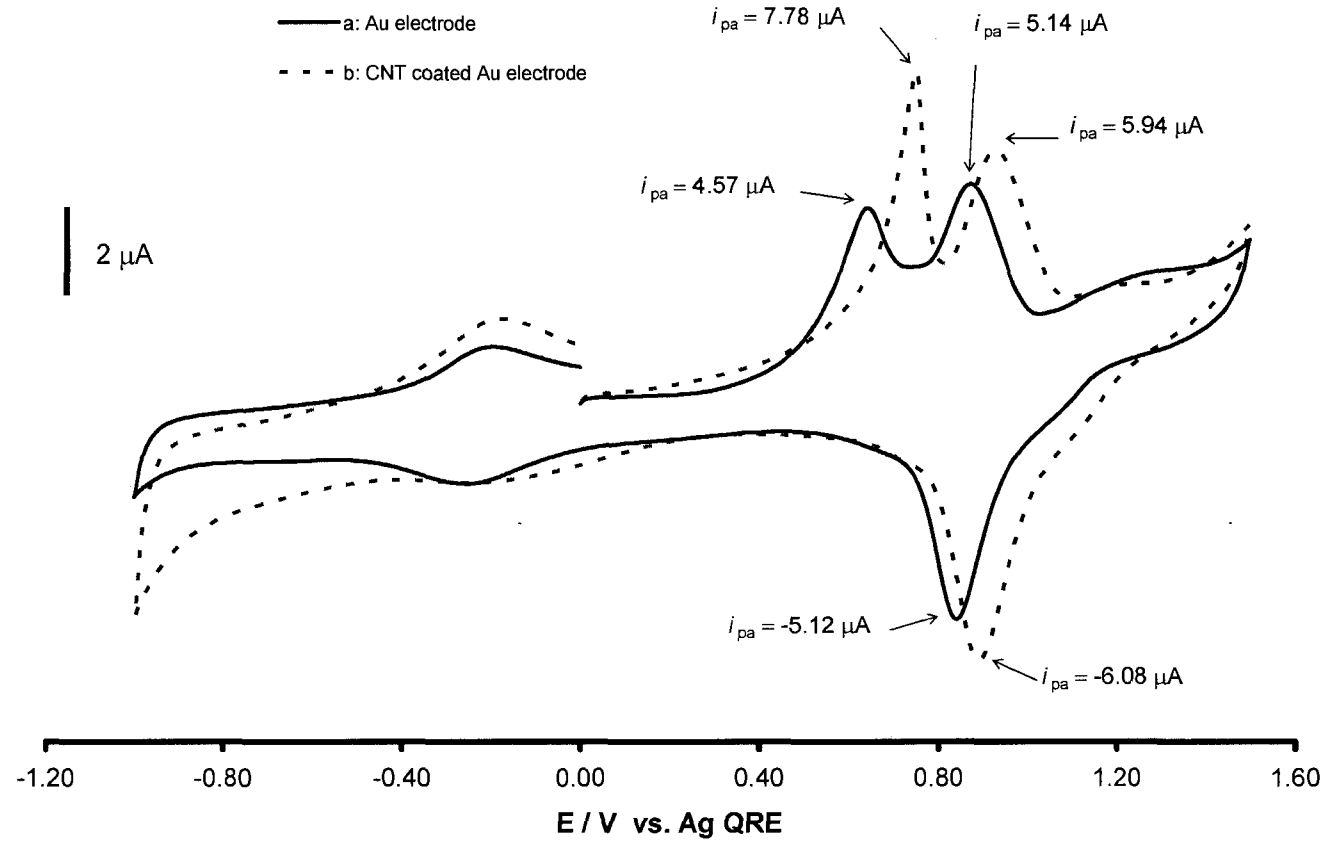

Figure 25. Comparison between the cyclic voltammograms of 50 μM $Fe(tpySCH_2\text{-}pyr)_2(OTF)_2$ at (a) a bare Au and (b) a CNT-coated Au electrode.

4. CONCLUSION

The resulting voltammograms of pyrene-free control compounds, $Fe(tpy)_2Cl_2$ and $Fe(tpySCH_3)_2(OTF)_2$ show no peak after the analyte in the cell has been replaced with fresh electrolyte, which shows that they did not adsorb on the electrode surface. The results were supported by scan rate studies of sweep rate dependence of peak current response. Well-resolved redox waves were observed after the solution of $Fe(tpySCH_2\text{-}pyr)_2(OTF)_2$ was replaced with fresh electrolyte, which suggests that $Fe(tpySCH_2\text{-}pyr)_2(OTF)_2$ molecules strongly adsorb on the electrode surface. The observation was also supported by scan rate studies.

It was also observed that the coverage of $Fe(tpySCH_2\text{-}pyr)_2(OTF)_2$ increased with increasing number of CV scans performed in the analyte solution. This suggests that $Fe(tpySCH_2\text{-}pyr)_2(OTF)_2$ polymerization occurs and that it is stimulated by CV scans. Without CV scanning, $Fe(tpySCH_2\text{-}pyr)_2(OTF)_2$ molecules physisorb on the electrode surface and show a submonolayer coverage on the electrode after immersing the electrode in 500μM solution for 10 minutes and rinsing with clean solvent, and the molecules remained on the surface of electrode but gradually desorb in clean electrolyte.

The experimental results also show that in comparison to the bare electrodes, CNT-coated electrodes give a larger current response indicating that the CNT coatings used increase the effective area for adsorption. Spectroelectrochemical analysis of $Fe(tpySCH_2\text{-}pyr)_2(OTF)_2$ shows a good fit to the ideal Nernstian response. Reversbility of the reaction was implied and a small electroinactive region was also observed. Experiments done at Au electrodes show more complicated results than the GC electrode

which may be related to the interaction between sulfur and Au, but the actual causes remain unclear.

REFERENCES

1. Collins, P. G.; Avouris, P. *Scientific American* **2000**, *283*, 62-69.

2. Dresselhaus, M. S.; Dresselhaus, G.; Saito, R. *Carbon* **1995**, *33*, 883-891.

3. Yakobson, B. I.; Bernholc, J. *Phys. Rev. Lett.* **1996**, *76*, 2511-2514.

4. Berber, S.; Kwon, Y. K.; Tomanek, D. *Phy. Rev. Lett.* **2000**, *84*, 4613-4616.

5. Tans, S. J.; Verschueren, A. R. M.; Dekker, C. *Nature* **1998**, *393*, 49-52.

6. Martel, R.; Schmidt, T.; Shea, H. R.; Hertel, T.; Avouris, P. *Appl. Phys. Lett.* **1998**, *73*, 2447-2449.

7. Zhu, W.; Bower, C.; Zhou, O.; Kochanski, G.; Jin, S. *Appl. Phys. Lett.* **1999**, *75*, 873-875.

8. Cadek, M.; Coleman, J. N.; Ryan, K. P.; Nicolosi, V.; Bister, G.; Fonseca, A.; Nagy, J. B.; Szostak, K.; Beguin, F.; Blau, W. J. *Nano Lett.* **2004**, *4*, 353-356.

9. Dillon, A. C.; Jones, K. M.; Bekkeclahl, T. A.; Kiang, C. K.; Bethune, B. S.; Heben, M. J. *Nature* **1997**, *386*, 377-379.

10. Woolley, A. T.; Cheung, C. L.; Hafner, J. H.; Lieber, C. M. *Chemistry & Biology* **2000**, *7*, R193-R204.

11. Tu, Y.; Lin, Y.; Yantasee, W.; Ren, Z. *Electroanalysis* **2005**, *17*, 79-84.

12. Gooding, J. J. *Electrochimica Acta* **2005**, *50*, 3049-3060.

13. Wildgoose, G. G; Banks, C. E.; Leventis, H. C.; Compton, R. G. *Microchim Acta* **2006**, *152*, 187-216.

14. Kong, J.; Franklin, N. R.; Zhou, C.; Chapline, M. G.; Peng, S.; Cho, K.; Dai, H. *Science* **2000**, *287*, 622-625.

15. Murray, R. W.; Ewing, A. G.; Durst, R. A. *Anal. Chem.* **1987**, *59*, 379A-390A.

16. Bard, A. J.; Faulkner, L. R. *Electrochemical Methods: Fundamentals and Applications*, 2nd ed.; John Wiley & Sons: New York, 2001.

17. Wang, J. *Analytical Electrochemistry*, 2nd ed; Wiley-VCH: New York, 2001.

18. Heyrovsky, J. *Chem. Listy.* **1922**, *16*, 256-264.

19. Izutsu, K. *Electrochemistry in Nonaqueous Solutions*; Wiley-VCH: Weinheim, Germany, 2002.

20. Brown, A. P.; Anson, F. C. *Anal. Chem.* **1977**, *49*, 1589-1595.

21. Zhang, L.; Jiang, X.; Wang, E.; Dong, S. *Biosensors and Bioelectronics* **2005**, *21*, 337-345.

22. Wang, J.; Li, M.; Shi, Z.; Li, N.; Gu, Z. *Electrochimica Acta* **2001**, *47*, 651-657.

23. Britto, P. J.; Santhanam, K. S. V.; Ajayan, P. M. *Bioelectrochemistry and Bioenergetics* **1996**, *41*, 121-125.

24. Waltman, R. J.; Bargon, J. *J. Electroanal. Chem.* **1985**, *194*, 49-62.